Journal of Natural Gas Science and Engineering 39 (2017) 143–160

Contents lists available at ScienceDirect

Journal of Natural Gas Science and Engineering

journal homepage: www.elsevier.com/locate/jngse

Review Article

Cleat-scale characterisation of coal: An overview

Peyman Mostaghimi*, Ryan T. Armstrong, Alireza Gerami, Yibing Hu, Yu Jing, Fatemeh Kamali, Min Liu, Zhishang Liu, Xiao Lu, Hamed L. Ramandi, Ali Zamani, Yulai Zhang

MUTRIS Research Group, School of Petroleum Engineering, The University of New South Wales, NSW 2052, Australia

ARTICLE INFO

Article history:
Received 20 September 2016
Received in revised form
27 January 2017
Accepted 28 January 2017
Available online 3 February 2017

Keywords:
Coal seam gas
Coalbed methane
Coal cleats
Pore-scale modelling
Micro-CT imaging
Image analysis

ABSTRACT

This paper reviews recent developments on the cleat-scale characterisation of coal. Novel micro-CT imaging and image calibration methods are described. The application of micro-CT imaging for studying diffusion processes in ultralow permeability media is shown. The extraction of statistical information from micro-CT images to reconstruct cleats are demonstrated. The developments of microfluidic methods for understanding complex displacement mechanisms in coal seams and variation of coal contact angles are described. We explain numerical methods for prediction of petrophysical properties from micro-CT images and discuss limitations when dealing with coal. The paper concludes by addressing the challenges for microscale coal characterisation.

Contents

1. Introduction

Coal seam gas (CSG), which is also commonly known as coalbed methane (CBM), is the natural gas trapped in unconventional

* Corresponding author.
E-mail address: peyman@unsw.edu.au (P. Mostaghimi).

http://dx.doi.org/10.1016/j.jngse.2017.01.025
1875-5100/

coalbeds. It had been causing outbursts and explosions during coal mining processes for over a century. The gas in coal seams was vented by airways to eliminate hazards until it began to be of economic interest in the 1970s' oil crisis in the USA (Flores, 1998). Nowadays, CSG has been commercially extracted in many countries, mainly Australia, Canada, China, India, Poland and USA (Gunter et al., 1997; Kotarba, 2001; Narasimhan et al., 1998; Shengchu et al., 2009; Towler et al., 2016). Recently, there have been investments in CSG recovery in other countries including Indonesia and Russia. CSG reservoirs have also been considered to be used for sequestering carbon dioxide (Gale and Freund, 2001; Tsotsis et al., 2004; Wei et al., 2010).

Several factors make displacements in coalbeds different to conventional hydrocarbon reservoirs. These differences are associated with specific physical mechanisms occurring during methane recovery as well as the formation of the CSG reservoirs. (i) In a conventional reservoir, hydrocarbons are mostly generated in shales or limestones, also known as source rocks, and migrate to shallower depths where it is trapped by a cap rock (Cossé, 1993). However, in CSG reservoirs, coal acts as both source and reservoir rock such that the gas initially formed during the coalification processes is stored there (Clarkson and Bustin, 1999; Seidle, 2011). (ii) Coal as a reservoir rock is of low porosity (0.5–2.5%) (Gash et al., 1992; Laubach et al., 1998) with a wide range of permeability (0.1–100 mD). (iii) Another difference is related to the presence of gas in conventional reservoirs where it exists mostly in free state, i.e. the gas is free to move in the pore spaces. For CSG reservoirs, 98% of gas is stored in the coal matrix and is released by sorption mechanisms during dewatering and production processes (Gray, 1987; Meng et al., 2014). This introduces new physics into the production mechanisms from these resources. (iv) The production profiles in conventional gas reservoirs are also different in comparison with CSG reservoirs. The initial production from a conventional gas reservoir consists of mostly gas with negligible amount of water. As the production continues, the fraction of water produced increases while the gas production decreases. However, in CSG reservoirs, production is initiated by dewatering, which releases the gas adsorbed to coal surfaces. This makes the production profile different to that of a conventional reservoir (Moore, 2012). (v) The pore space morphological properties are also unique in coal such that, at the pore scale, an orthogonal fracture system provides pathways for fluid flow. The coal fracture system is known as “cleats”, which commonly occur in two main sets of sub-parallel fractures; face cleats and butt cleats. In most circumstances, face cleats are formed first during coalification, whereas butt cleats occur later and terminate at face cleats, resulting from the relaxation of the original stress field (Gao et al., 2014; Scholtès et al., 2011). This is in contrast to conventional sandstone gas reservoirs where the pore space is a granular medium formed through processes including sedimentation, compaction, and diagenesis. The unique pore space geometry of coal with cleat apertures less than 0.1 mm (Laubach et al., 1998) as well as the brittle textures of coal cause difficulties in the use of traditional laboratory measurements on coal cores. (vi) Coal permeability varies dramatically during reservoir production as coal is highly deformable and the cleat system deforms due to change of reservoir pressure and sorption mechanisms (Pan and Connell, 2012).

Over the last two decades, pore-scale imaging and modelling has received increasing attention for the understanding of displacement phenomena in reservoir rocks (Blunt, 2001; Blunt et al., 2013). It has offered oil and gas industries novel solutions for prediction of petrophysical properties of rocks that are difficult or in some cases impossible to obtain through applying conventional laboratory routines. Pore-scale modelling of rocks has also provided several new research opportunities to answer many questions on flow, transport, and reaction in porous media (Armstrong et al., 2016; Bijeljic and Blunt, 2006; Bijeljic et al., 2011; Joekar-Niasar and Hassanizadeh, 2012; Liu and Mostaghimi, 2017; Mostaghimi et al., 2012, 2016b; Tansey and Balhoff, 2016). In this paper, we review some recent developments of pore-scale imaging and modelling in the CSG context and demonstrate the unconventional challenges that are faced. Even though, many of the methods discussed are now a standard tool for managing and analysing conventional hydrocarbon reservoirs, they have not been fully translated to unconventional resources and in particular for the CSG industry. Due to the specific pore structure of coal cores as well as different multiphysics occurring during gas production, new challenges are to be faced for the micro-scale characterisation of coals. This paper is not intended to review all of the different applications of pore-scale imaging and modelling of coal. It is mainly focused on a few comprehensive applications of pore-scale analysis in coalbeds of interest to the authors. These include wet and dry imaging, image calibration, statistical analysis of cleat systems, diffusion modelling, coal wettability and microfluidics that have been developed mostly over the last few years. Fig. 1 illustrates the organisation of this paper.

2. Micro-CT imaging

2.1. X-ray imaging and processing

X-ray micro-computed tomography (micro-CT) is a non-

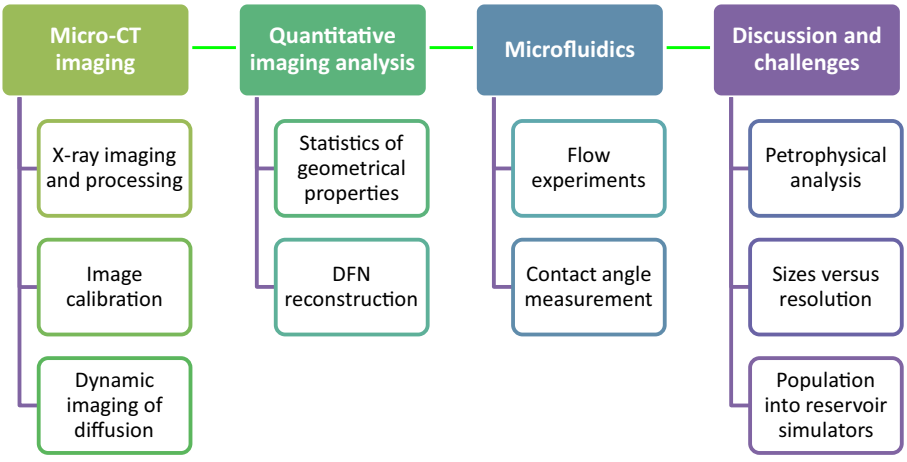

Fig. 1. An overview of the contents provided in this paper.

destructive method that has been used for capturing the pore space geometries of a variety of reservoir rocks (Armstrong et al., 2014; Golab et al., 2010; Johns et al., 1993; Ketcham and Carlson, 2001; Menke et al., 2015; Qajar et al., 2013; Saadatfar et al., 2005; Wildenschild et al., 2002). The basic elements of a micro-CT scanner are an X-ray source, a sample stage and a detector unit. The X-ray source is fixed while the detector and stage move to alter the distance between the sample and detector to adjust the magnification. The stage may also be able to move vertically while rotating, enabling acquisition of data along a helical scanning trajectory (Varslot et al., 2012). During micro-CT imaging, a polychromatic beam is emitted from the X-ray source. This beam passes through attenuating filters, prior to passing through the sample, to minimise imaging artifacts. Within the sample the filtered beam is absorbed, scattered, diffracted, refracted, or transmitted while passing through materials of different densities. Then, an array X-ray detector collects the beam and measures the extent to which the X-ray signal has been attenuated. The collected data, which characterises the cumulative attenuation of the X-ray beam are processed based on reconstruction algorithms to generate a 3D image of the sample (Hsieh, 2009). The resulting image is displayed as a grey-scale map in which each data point, referred to as voxel, representing the effective X-ray attenuation coefficient of the sample composition.

The pore size in coal ranges widely and analysing its distribution is crucial for coal characterisation. Rather than micro-CT imaging, there are other techniques to obtain the pore size distribution of coal. These include Nuclear Magnetic Resonance (NMR) imaging, and Mercury Intrusion Porosimetry (MIP). For capabilities of these two methods and a comparison between them, we refer to Yao and Liu (2012). Micro-CT imaging has been applied to coal for a variety of purposes. Bossie-Codreanu et al. (2004), Cai et al. (2014), De Kock et al. (2015), Espinoza et al. (2016), Heriawan and Koike (2015), Mazumder et al. (2006), Montemagno and Pyrak-Nolte (1999), Mostaghimi et al. (2015a), Naudé et al. (2013), Ramandi et al. (2015, 2016b), Van Geet and Swennen (2001), Wolf et al. (2008) and Yao et al. (2009) have developed frameworks for measurement of coal fracture aperture, length, distribution, spacing and direction. They related these attributes to coal rank, lithotype and the stress regime of studied region. Karacan and Okandan (2001), Karacan (2003), Karacan and Mitchell (2003), Karacan (2007) and He et al. (2010) have developed methods for measuring the amount and rate of adsorption as well as kinetics of gas sorption in coal. Also, they characterised transport and storage characteristics of different lithotypes during gas adsorption or sequestration of carbon dioxide. Simons and Swennen (1997), Van Geet et al. (2001), Verhelst et al. (1996) and Yao et al. (2009) have measured coal matrix constituents distributions. They have established cross-correlations between measured tomo-densities and different coal constituents. Yao et al. (2009, 2010), Li et al. (2012), Yu et al. (2012), Naudé et al. (2013), Vega et al. (2014), Mayo et al. (2015), Pant et al. (2015), Liu et al. (2017), and Zhang et al. (2016a) characterised coal pore attributes. They measured coal porosity using dual scan and segmentation methods and compared the image-based porosity results with experimental results. They analysed coal pore structure and determined number of isolated pores and pore size distributions. Moreover, they have developed 3D models of the pore network for petrophysical analyses. Golab et al. (2013), Ramandi et al. (2015, 2016b) have mapped the 3D distribution of minerals in coal and compared the results to XRD, optical, SEM-EDX and QEMSCAN data. They have studied the relationship between mineral content and coal permeability. Mathews et al. (2011) have analysed the extent of drying-induced transitions in coal. They have observed induced cracking, shrinkage and aperture size changes during moisture loss. Karacan (2007), Pone et al. (2009, 2010), Mao et al. (2015), Feng et al. (2016), Zhang et al. (2016b, 2016c) studied coal deformation and variation of pore structure due to swelling. They discussed the relationship between the permeability reduction and coal swelling. Also, they observed fracturing of the minerals due to swelling and measured the volumetric strains. They related coal swelling to pore, fracture, lithotype and mineral types.

The aforementioned studies have significantly advanced pore-scale imaging and modelling methods for coal characterisation. However, representative quantitative data are still limited due to the multiscale heterogeneity of the coal cleat system and its unconventional nature. In addition, due to the existence of microporosity in coal, full characterisation of coal pores is not feasible with single resolution imaging. In a recent study, Ramandi et al. (2016b) used a custom-built helical micro-CT scanner for imaging of a coal sample from Bowen Basin, Australia (vitrinite reflectance = 1.15%). The sample was first imaged at as-received condition, i.e. dry imaging. The dry image was the key image for mineral mapping and generation of calibration curves. Then, the sample was saturated with an X-ray attenuating fluid, which has a high level of attenuation towards X-rays. The saturated sample was then re-scanned to provide the wet image, in which all of the fractures available to the brine were displayed with higher grey-scale values, generally similar to minerals. Dry and wet images were then registered to each other using the computational method explained in Latham et al. (2008). The method brings the images into geometric alignment and provides images with identical dimensions. Then a difference image was obtained from subtraction of the registered dry and wet images. The difference image highlights all of the fluid-penetrated fractures and is the key image for the fracture segmentation (Fig. 2).

To enhance the quality of acquired images, commonly several filters are employed. Ramandi et al. (2016b) applied nonlinear anisotropic diffusion and unsharp mask filters to improve the quality of coal images. The anisotropic diffusion filter reduces the noise improving the signal-to-noise ratio of tomographic images while preserving edges. The unsharp mask sharpens the edges without overly intensifying the noise (Sheppard et al., 2004). Schlüter et al. (2014) provides a comprehensive review of the image filtering and segmentation techniques. When filtering micro-CT data the image will loose some degree of information and thus this step should be undertaken with caution. Image filtering is one of the very first steps in the digital coal characterisation and is possibly also the most important.

Image segmentation is the process of partitioning of the grey-scale image into unique phases. Coal segmentation means deciding to which phase, minerals, macerals and fractures, each voxel belongs to. To achieve a satisfactory segmentation result, Ramandi et al. (2016b) employed an advanced method based on a combination of the watershed method (Vincent and Soille, 1991) and active contour methods, termed converging active contours (CAC). CAC uses intensity information and gradient simultaneously (Sakellariou et al., 2007; Sheppard et al., 2004). To initialise the CAC algorithm, two user-defined threshold values that are chosen according to visual inspection of the grey-scale image histogram are considered. Voxels with grey-scale values higher than the upper threshold are labelled as solid phase and those below the lower threshold are labelled as pore. The values between the upper and lower thresholds are labelled as boundary regions. The image intensity gradient is used at boundary regions to detect the exact interfaces between phases (Sakellariou et al., 2007; Sheppard et al., 2004). The algorithm proceeds by simultaneously converging the boundaries of the solid and void regions toward each other until boundaries touch (Schlüter et al., 2014). The speed at which the boundaries converge varies spatially and temporally, depending on the local gradient and the distance of the local voxel value to the

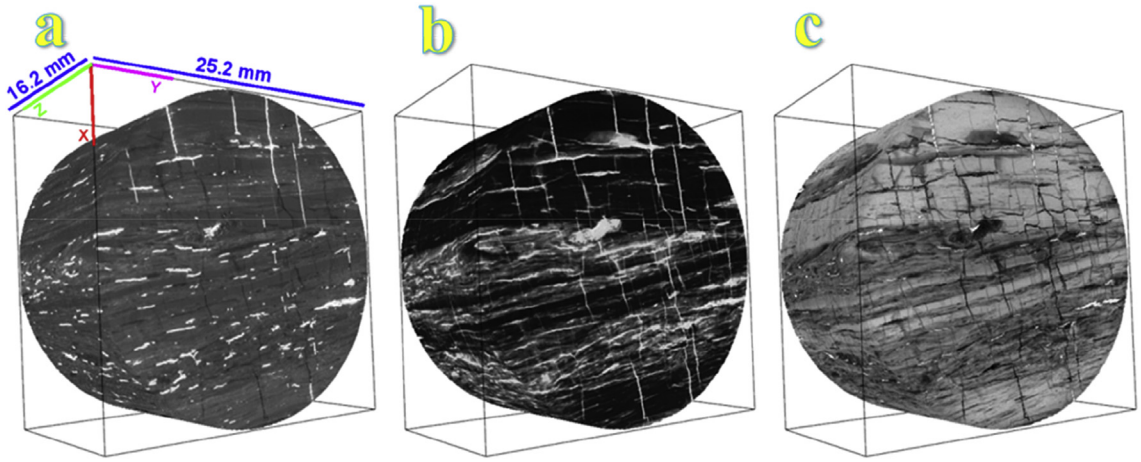

Fig. 2. (a) A registered dry micro-CT image of a coal sample (black = pores and fractures, grey = macerals and white = minerals), (b) the same sample after saturation with X-ray attenuating fluid (white = minerals and saturated pores and fractures and black = macerals), (c) the difference image of the same sample (black = pores and fractures, grey = macerals and white = minerals).

mean voxel value of its corresponding phase (Schlüter et al., 2014). Sub-resolution pores and fractures can contain similar grey-scale values and make the image segmentation more challenging. Ramandi et al. (2017) initially segmented the digital image of coal using CAC. Then, they applied erosion and dilation operations to the segmented image to partition the sub-resolution fractures from sub resolution pores (Fig. 3).

2.2. Image calibration

The coal cleats visualised with micro-CT imaging, when using a contrast agent, are often smaller than they appear and thus cannot be accurately resolved. Several methods based on different attributes of the local gradient in voxel values from the raw and/or filtered images are developed to generate a calibration curve for measuring the aperture size from digital images. These attributes include peak height (PH) (Mazumder et al., 2006; Vandersteen et al., 2003; Verhelst et al., 1995), full-width-half-maximum (FWHM) (Peyton et al., 1992), and missing attenuation (MA) (Johns et al., 1993; Mazumder et al., 2006; Vandersteen et al., 2003). These methods require at least two sets of micro-CT images; one for imaging fractures of known dimensions and another for the sample of interest. Since the proposed calibration curves disregard the variation of the attenuation coefficient with imaging conditions, measuring the aperture sizes in the image of interest using this type of calibration curve results in potential measurement errors. Ramandi et al. (2016a) proposed a calibration method in which the requirement for two sets of micro-CT images is eliminated. In their method, after micro-CT imaging, the sample is prepared for scanning electron microscopy (SEM) imaging. Then, the SEM images are obtained and registered to the corresponding slices from the micro-CT image (Latham et al., 2008). Afterwards, they used the registered SEM images as the ground-truth fracture aperture measurement to find the point spread function (PSF) of the micro-CT image. Then, a calibration curve is derived by plotting the peak height value of several aperture profiles acquired from the micro-CT image against the aperture size measured using the method explained by Ketcham et al. (2010) (Fig. 4). This calibration curve delivers a direct relationship between the true fracture aperture width and the grey-scale value at the midpoint of a fracture. The overall method is shown in Fig. 4.

Ramandi et al. (2017) used the calibration curve to adjust aperture sizes in a 3D micro-CT image for generating a binary image that can be used for flow simulation. To perform this, they up-sampled the segmented and original raw images using Catmull-Rom interpolation (Catmull and Rom, 1974), to obtain images with ¼ the original voxel size. Ketcham et al. (2010) found that fracture apertures ¼ of the original voxel resolution could be measured using the proposed PSF method. Then, the segmented fracture network was thinned to a single voxel to provide a fracture

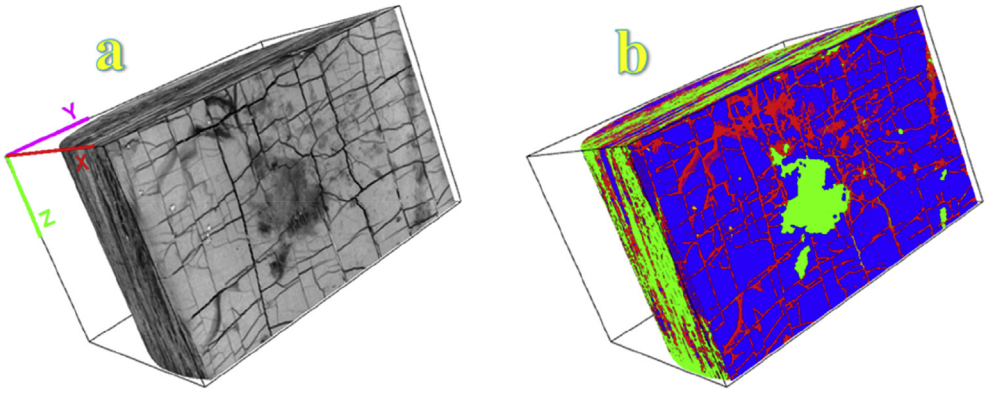

Fig. 3. (a) The difference image (black = fractures and pores, grey = macerals and white = minerals), (b) the segmented image (red = fractures, green = sub-resolution pores, blue = macerals and orange = minerals). (For interpretation of the references to colour in this figure, the reader is referred to the web version of this article.)

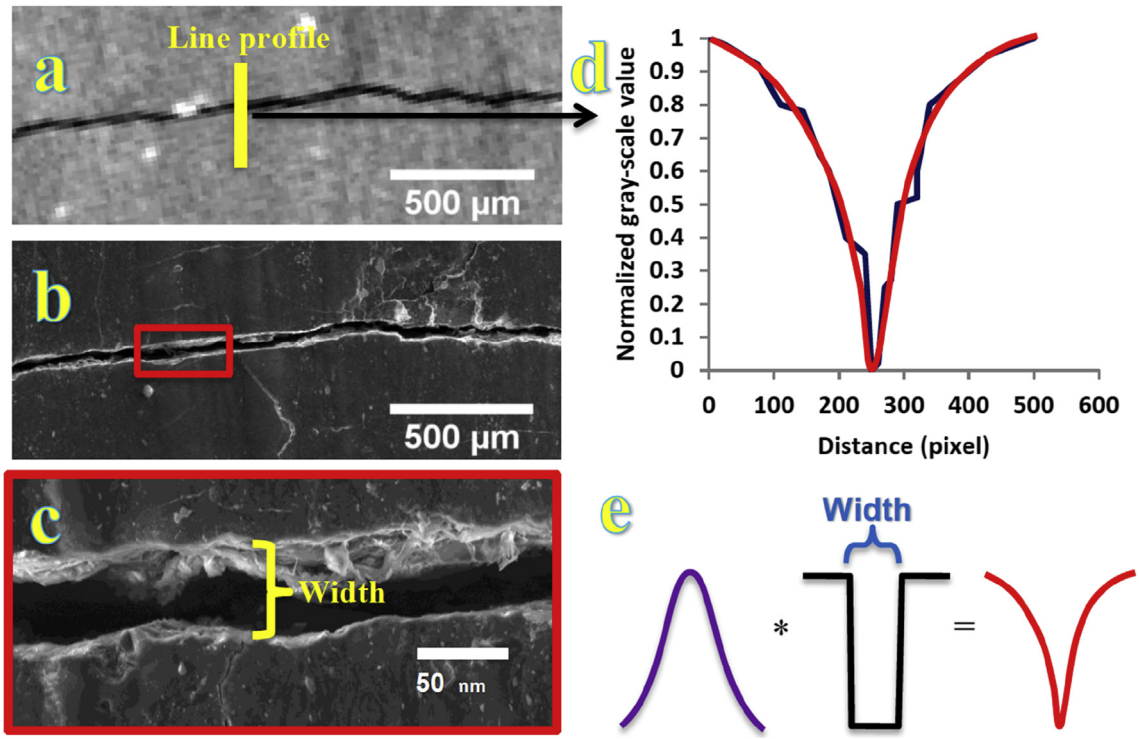

Fig. 4. (a) A dry registered micro-CT slice, (b) the registered SEM image from the same region, (c) enlarged portion of the highlighted region in the registered SEM image (b), (d) the line profile (black) and matched curve (red) of the fracture in micro-CT image, (e) a schematic of the aperture measurement method using PSF (purple), box function (black) and matched curve. (For interpretation of the references to colour in this figure, the reader is referred to the web version of this article.)

network skeleton. This thinned fracture network was consequently used to extract the fracture mid-point values from the grey-scale up-sampled raw image. The extracted grey-scale values were, then, converted to true aperture sizes using a calibration curve. This provided a weighted thinned fracture network that contains the true aperture sizes. This was then passed to an adjustment algorithm to generate a binary image by opening the weighted thinned fracture network according to the true aperture sizes. The resulting binary image (Fig. 5) that contains a structure representative of the sample with calibrated aperture widths was then used for numerical and statistical analyses. The main disadvantage of this method is that the resulting calibrated image is 4 times larger than the original image, which requires high-performance computing to simulate flow.

2.3. Dynamic imaging of diffusion processes

Gas sorption and diffusion in the coal matrix is an important

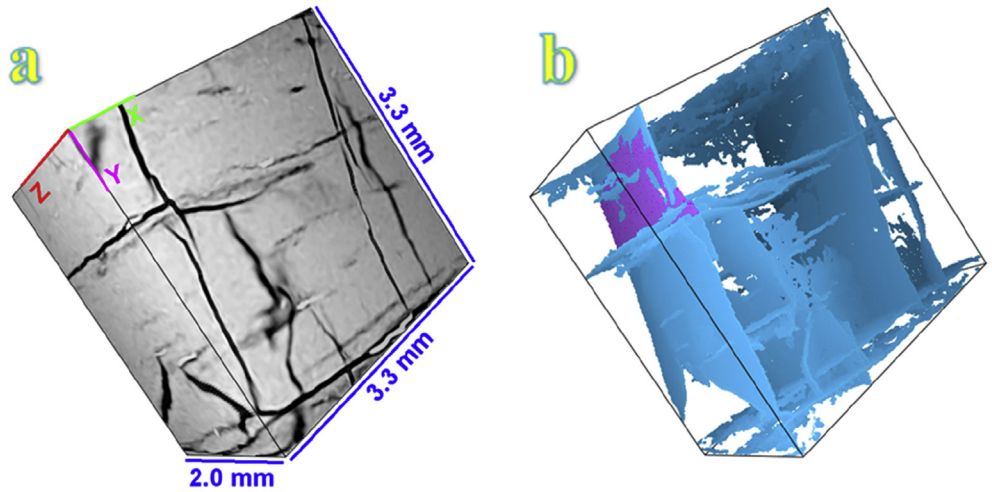

Fig. 5. 3D visualisation of coal cleat system:(a) the difference image of the sample (black = pores and fractures, gray = macerals and white = minerals), (b) the connected fracture network of the sample before and after calibration (magenta region is the only connected region in the non-calibrated image while the entire network (magenta and blue) presents the connected network of the calibrated image). Animation is available at http://www.mutris.unsw.edu.au. (For interpretation of the references to colour in this figure, the reader is referred to the web version of this article.)

factor influencing the production profile and recovery factor of CSG reservoirs (Pillalamarry et al., 2011) and thus several studies have been focused to characterise these mechanisms in coal. The diffusion processes within coal include three key mechanisms; bulk diffusion, Knudsen diffusion and surface diffusion (King et al., 1986). A study on an Australian coal found that the methane diffusivity increases with the decrease of moisture content and the increase of pressure (Pan et al., 2010). Another study on Illinois basin coal suggested that in coalbeds, the diffusion coefficient of methane varies with time and can be represented by a "dual model" with constant diffusion coefficient at high pressure and increasing diffusion coefficient at low pressures after significant methane desorption (Pillalamarry et al., 2011). Most of the previous studies employed a diffusion experiment approach, in which gas sorption experiments on coal were carried out and then analysed by unipore or bidisperse models to determine the diffusion coefficients (Clarkson and Bustin, 1999; Pan et al., 2010; Ruckenstein et al., 1971). Micro-CT imaging can be used for the determination of diffusion processes in porous media, as it monitors the diffusion within the sample without any interference to the dynamic process or any damage to the sample (Fogden et al., 2015). Most of the micro-CT applications for measuring diffusion coefficients have focused on sandstones and shales (Cavé et al., 2009; Guerrero Aconcha and Kantzas, 2009; Liu et al., 2016; Polak et al., 2003; Tidwell et al., 2000). Vega et al. (2014) showed an example of using coal for visualising diffusion processes at the pore scale.

Herein, a quantitatively study of diffusion in shales using micro-CT imaging is presented to illustrate the potential of micro-CT for diffusion studies in low-permeability domains. The similarities between coal seams and shale gas reservoirs, including existence of a dual porosity system, diffusion in matrix and Darcy flow in cleats/fractures, sorption/desorption of gas, and ultralow permeability in matrix make the developed method applicable to coal. We report measurements of the 1D bulk diffusion coefficient of a shale sample with diameter of 12 mm, using liquid diiodomethane (CH_2I_2) as a tracer. A section of the sample, 8.8 mm in height, is continuously circularly scanned after the whole sample is submerged into toluene, which is miscible with CH_2I_2 and X-ray transparent. The diffusion process is triggered as CH_2I_2 molecules diffusing into surrounding toluene and this results in a continuous loss of attenuation of the sample. As each scan will produce one image, the diffusion process is transferred into a temporally discrete process by micro-CT images with each image representing an attenuating state that can be converted to a concentration state. These images are referred as "diffusion images". All images are 3D with a voxel size of 9.6 μm, so each image has a total number of 1250 × 1250 × 920 voxels (Fogden et al., 2015). Following the image processing and registration, the following equation is used to calculate tracer concentration based on the linear relationship between CT number and density of the scanned object (Cavé et al., 2009; Wildenschild and Sheppard, 2013):

$$C_{x,y,z,t} = \frac{CT_{diff(x,y,z,t)} - CT_{dry(x,y,z)}}{CT_{wet(x,y,z)} - CT_{dry(x,y,z)}} \quad (1)$$

where $CT_{diff(x,y,z,t)}$ is the CT number at location (x, y, z) of the diffusion image at time t and $CT_{wet(x,y,z)}$ and $CT_{dry(x,y,z)}$ are the CT numbers at location (x, y, z) of the wet and dry images, respectively. From Eq. (1) concentration of tracer at each voxel of the image at each discrete time is scaled to range between 0 and 1. For bulk diffusion coefficient, the sample is treated as homogeneous with a uniform diffusion coefficient. It is measured by fitting the 1D concentration profile along the direction of diffusion, which is calculated based on Fick's second law (Eq. (2), to that calculated from Eq. (1) by varying the diffusion coefficient until a match is found (Cavé et al., 2009; Tidwell et al., 2000). The diffusion equation is the following

$$\frac{dZ}{dt} = \frac{D_e}{\varepsilon}\frac{d^2Z}{dx^2} \quad (2)$$

where Z is concentration, D_e is the effective diffusion coefficient, and ε is average porosity.

Fig. 6 shows three 2D concentration distributions of the same cross section of the sample at experimental times of 15 h, 48 h and 90 h. Micro-CT imaging offers unique visualisation of the dynamic diffusion processes in low-permeability porous media. In addition, the local variation of the diffusion process can be captured by the images. It is clearly shown that on the right side of the sample there is faster diffusion than other areas, indicated by the deeper propagation of the dark colour on the right side of the sample.

A radial concentration profile is measured from the location as indicated by the blue line in Fig. 6. For this particular location, the best-fit bulk effective diffusion coefficient was determined, which is found by comparing the squared difference between theoretical and experimental data. The fitting outcome is shown in Fig. 7 and the result is near the shale diffusion coefficient reported in Cavé et al. (2009). In addition, Fig. 7 demonstrates that assuming a uniform diffusion coefficient may provide an acceptable estimation of the diffusion coefficient since the local heterogeneity of the diffusion coefficient is ignored. For example, the zone between 250 and 350 pixels has higher diffusion coefficients, as the concentration data are much lower than the theoretical values. In addition, the directionality of the diffusion coefficient has been excluded. For example, if a fracture exists below the location of the interest, then vertical diffusion in the direction would be larger than radial diffusion due to the larger concentration gradient.

Due to the limitations of 1D bulk diffusivity measurements, more comprehensive studies on diffusion in coal using micro-CT imaging are planned by the authors, in which the diffusion in all directions will be accounted for in the mathematical model and diffusivity at each voxel will be calculated. We treat each voxel of the image as a continuum scale and calculate the local diffusive flux and concentration gradient, and then the directional local diffusivity can be measured. Although this methodology may not be directly correlated to different scales of pores of a coal, as some pores are only in nanometre scales (Clarkson and Bustin, 1999) that is beyond the ability of micro-CT imaging given a centimetre scale sample, it provides a way to study the diffusion characteristics from a core scale field of view. Also, from local diffusivity measurements, we are able to infer matrix tortuosity and constrictivity and how these values vary over a full core plug and/or from sample to sample. These findings, together with the local variation of the diffusion coefficient can be good indicators of local heterogeneity of the coal matrix. The proposed future studies would provide more insights into the role of diffusion in gas production from CSG reservoirs.

3. Quantitative image analysis

3.1. Statistics of cleat geometrical properties

Micro-CT images of coal are difficult for direct numerical simulation because of problems that arise during image segmentation. For example, resolution limitations and image segmentation errors cause bottleneck features and non-conductive cleat networks, which subsequently induce numerical instabilities. Therefore, a discrete fracture network model (DFN) representing the micro-CT images can be constructed to circumvent these issues.

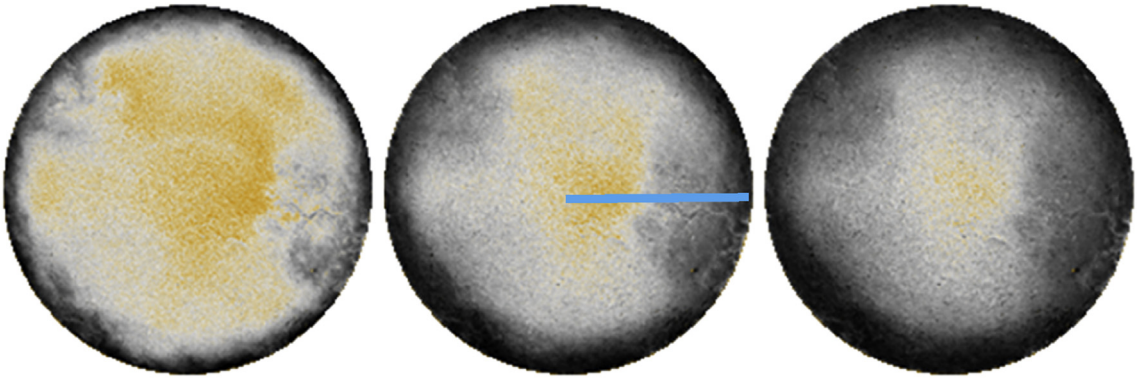

Fig. 6. Cross-sectional concentration distributions at experimental times of 15 h, 48 h and 90 h, from left to right; the location of 1D line profile readout is shown by a blue line. (For interpretation of the references to colour in this figure, the reader is referred to the web version of this article.)

DFN describes discrete fractures explicitly with identical geometrical properties. These properties include fracture orientation, length, aperture and density, and are assumed to be statistically distributed (Baecher et al., 1977; Cacas et al., 1990; Deisman et al., 2010; Gao et al., 2014; Lorig et al., 2015; Robertson, 1970; Scholtès et al., 2011; Yang et al., 2014).

To obtain the geometrical statistics of the coal cleat network at the core scale, quantitative image analysis methods on the segmented micro-CT images have been developed. Bossie-Codreanu et al. (2004) and (Mazumder et al., 2006) measured cleat density, spacing, orientations and aperture sizes using micro-CT scanning. They applied quantitative image analysis packages (e.g. Amira, QWIN, ImageJ, ICY) for measuring orientations and lengths of fractures. Orientation measurement was based on calculating the largest eigenvector of the structure tensors (Bigun et al., 2004; Jahne, 1993) and the length was determined by the number of voxels where the cleat extend. They developed an algorithm to measure cleat spacing such that a set of parallel lines perpendicular to the cleat angle were added to the micro-CT images. Then, line segments that were in connection from one cleat to another were measured, representing the spacing data. However, their measurement approach required manual editing because cleats intersect with each other and are oriented in various directions. Therefore, manual pre-processing of the micro-CT images was required prior to measurements. Intersecting face and butt cleat families were separated and measured for orientations and lengths and undesirable oriented cleats were suppressed for spacing measurement. This semi-automatic approach is not practical for hundreds or thousands of images. Jing et al. (2016) improved the coal micro-CT image analysis methods of statistical extraction in terms of both efficiency and accuracy. They developed an automatic cleat grouping algorithm to distinguish between face and butt cleats for subsequent image analysis. To be exact, cleats of each 2D slice of micro-CT data are firstly skeletonised to be one-voxel wide with a thinning algorithm (Lee et al., 1994). Then each voxel representing a fracture is tagged with 8 neighbours. Based on the direction in which the tagged cleat pixel extends, the cleats were classified into face cleat family and orthogonal butt cleat family, which were used to extract independent statistics (Fig. 8). With the procedure of cleat family classification, the statistics of orientation, length, spacing and aperture sizes can be extracted automatically (Fig. 9). The orientation is the angle between the eigenvector with largest eigenvalue of the structure tensor towards the x-axis, length refers to the number of voxels of each cleat in the skeletonised image, spacing is the distance between the Cartesian voxel positions of adjacent cleats, and aperture size is measured by determining the twice distance of the cleat wall to the central line.

Jing et al. (2017) further analysed the cleat surface topography to obtain roughness statistics. After cleat family classification, they labelled cleats and extracted opposite rough walls of each cleat for surface analysis. For the extracted 3D height profile of each surface, it consists of high-frequency small scale roughness profile, low-frequency waviness profile and the surface global trend, which is determined by the cleat orientation. To obtain the stationary roughness profile, they subtracted those non-stationary variations from the whole surface profile by applying a surface smoothing algorithm. Then the roughness profile was analysed in terms of vertical and horizontal variations. Vertical variation was described by the amplitude descriptors, which represented the distance above/below the mean plane of the surface. Two parameters were calculated, including arithmetic mean absolute deviation (R_a), and root mean square deviation (RMS). Horizontal variation was described by correlation length (β) which measured how quickly the surface decays along the mean plane.

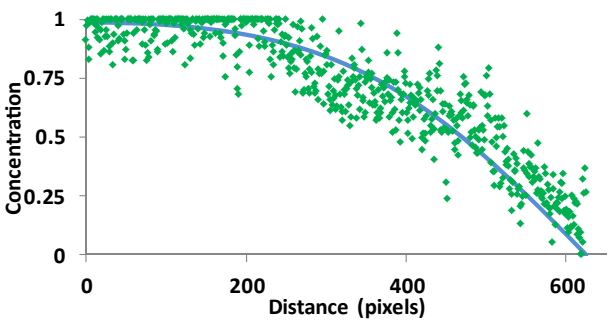

Fig. 7. Radial concentration profile (green dots) read from micro-CT images, compared with a best-fit curve (blue line) calculated from Eq. (2). (For interpretation of the references to colour in this figure, the reader is referred to the web version of this article.)

3.2. DFN reconstruction

Based on the statistical description of cleats, DFN models can be constructed. For a common DFN model, its fracture parameters are independently drawn from statistical distributions, known as the Poisson model (PM) (Maillot et al., 2014). But this is not applicable for coals, because for an organised cleat set the connectivity pattern mostly presents “T-junctions” between face and butt cleats, where face cleats are more extensive whereas butt cleats are shorter and terminate at face cleats (Gao et al., 2014; Scholtès et al., 2011). Nevertheless, most of the coal studies (Deisman et al., 2010; Gao

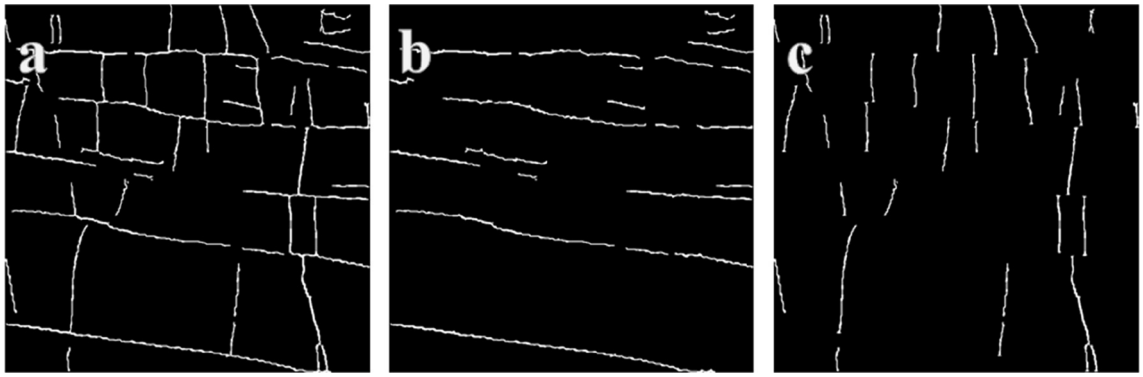

Fig. 8. An example of cleat family grouping: (a) full cleat network; (b) filtered face cleats; (c) filtered butt cleats.

et al., 2014; Lorig et al., 2015; Scholtès et al., 2011; Yang et al., 2014) disregarded the underlying connectivity of face and butt cleats, where DFN models were simply generated based on statistical descriptions only. Jing et al. (2016, 2017) developed novel DFN models specifically for coal cleat networks, which not only have geometrical statistics but also characterises the underlying cleat structure and surface roughness. In this method, the cleat reconstruction procedure involves generating face cleats first based on the measured statistics, and then butt cleats are produced randomly between the face cleats to form the "T-junctions". As shown in Fig. 10, the stochastic DFN model (Fig. 10b) captures the main structural features of the original coal cleat image (Fig. 10a) with identical geometrical statistics, i.e. the face cleats are thorough going and the butt cleats terminate at face cleats creating the characteristic "T-junction".

In order to investigate petrophysical properties of the DFN model, fast voxelisation processing (Jing et al., 2016) was applied to discretise the continuum geometry to provide binary files, on which the lattice Boltzmann method (Arns et al., 2005) can be utilised to solve for flow. Eight DFN realisations were stochastically generated with the Monte Carlo method (Chen et al., 2008) for numerical simulation. Results showed that the permeability and porosity of the DFN models are approximately 0.25 D and 4.04%, respectively, which are in agreement with measurements from the original micro-CT data. Furthermore, to study the scale effects of petrophysical properties, each realisation has 15 sub-samples. It is found that model domain size has a stronger effect on permeability than porosity (Fig. 11). Also, the developed DFN models assumed the cleats to be smooth and parallel planes, inducing the issues of overestimation of permeability. Therefore, roughness was further introduced to generate rough-walled DFN models (RW-DFN) (Jing et al., 2017). According to the measured roughness statistics, random rough surfaces that followed Gaussian distributions were constructed stochastically and then integrated with the conventional DFN models (Fig. 10c). By comparing reconstructed cleats from conventional DFN (Fig. 10e) and RW-DFN (Fig. 10f) with the real cleats from the original image (Fig. 10d), it can be seen that the RW-DFN preserves the local heterogeneity of original sample. By comparing with the permeability results of original micro-CT image (0.221D), it is shown that conventional DFNs over-estimate permeability (0.270D), while RW-DFNs provided more accurate results (0.201D), reducing the error approximately 25.1%–6.5%. Therefore, the issue of fracture transmissivity overestimation was alleviated by the RW-DFN model. Since the sample was scanned with no confining pressure, the permeability predicted is indeed higher than the permeability value at *in-situ* conditions. Also, the studied domain was cropped from a bright band of the coal sample, which had a well-developed cleat system giving higher permeability estimation. In future works, a pressure cell could be used for micro-CT imaging to provide digital cleat networks at *in situ* conditions providing more reliable permeability.

4. Microfluidics

4.1. Flow experiment

Recently, microfluidic methods have become popular in energy, oil and gas applications to study fluid flow in porous media. The application of this method has developed significantly after understanding the advantages of implementing microfluidics in obtaining experimental data of flow transport in conventional reservoirs. Joseph et al. (2013) and Xu et al. (2014) studied permeability in a microfluidic porous medium and obtained relationships between permeability and effective porosity. Oil production in water flooding processes in random networks were studied, and the effect of pore size distribution and matrix geometry on displacement efficiency was explored by Xu et al. (2014). Gunda et al. (2011) fabricated a microfluidic chip with a simplified network of pores and throats, derived from SEM images of rock samples. They measured oil recovery, which mimics the standard water flooding processes. Relative permeability was also studied by Avraam and Payatakes (1999) for steady-state flow in a network designed with a matrix of squares. Other studies employed Bitumen (a heavy oil mostly stored in Canadian and Middle Eastern reservoirs) in a micromodel and studied the displacement after injecting carbon dioxide. Song et al. (2014) used a microfluidic chip fabricated from calcite rock to study acid injection and reactive transport. They visualised interactions between the pore network matrix and acidified fluid in this set of experiments.

Very few studies have employed microfluidics for understanding and measuring displacement in coal seams. Mahoney et al. (2015a) explored the effect of rank and lithotype on coal wettability by fabricating a coal microfluidic chip. They stated that coal wettability is not only dependent on pore pressure and reservoir condition, but also varied for different coal ranks and compositions. Mahoney et al. (2015b) investigated a set of methods for creating micro-channels on a coal surface replicating natural cleats in CSG reservoirs. They concluded that reactive ion etching (RIE) and laser etching can generate cleat geometries that meet the width, depth and shape criteria (Mahoney et al., 2015b). Multiphase flow transport through a straight channel, etched on coal surface was analysed and visualised by Mahoney et al. (2015b). Gerami et al. (2016) developed a microfluidic chip based on coal cleat geometry. Micro-CT imaging was used to capture the cleat structure of a coal sample and microfluidic fabrication techniques were implemented to transfer the cleat network to a Polydimethylsiloxane (PDMS) chip.

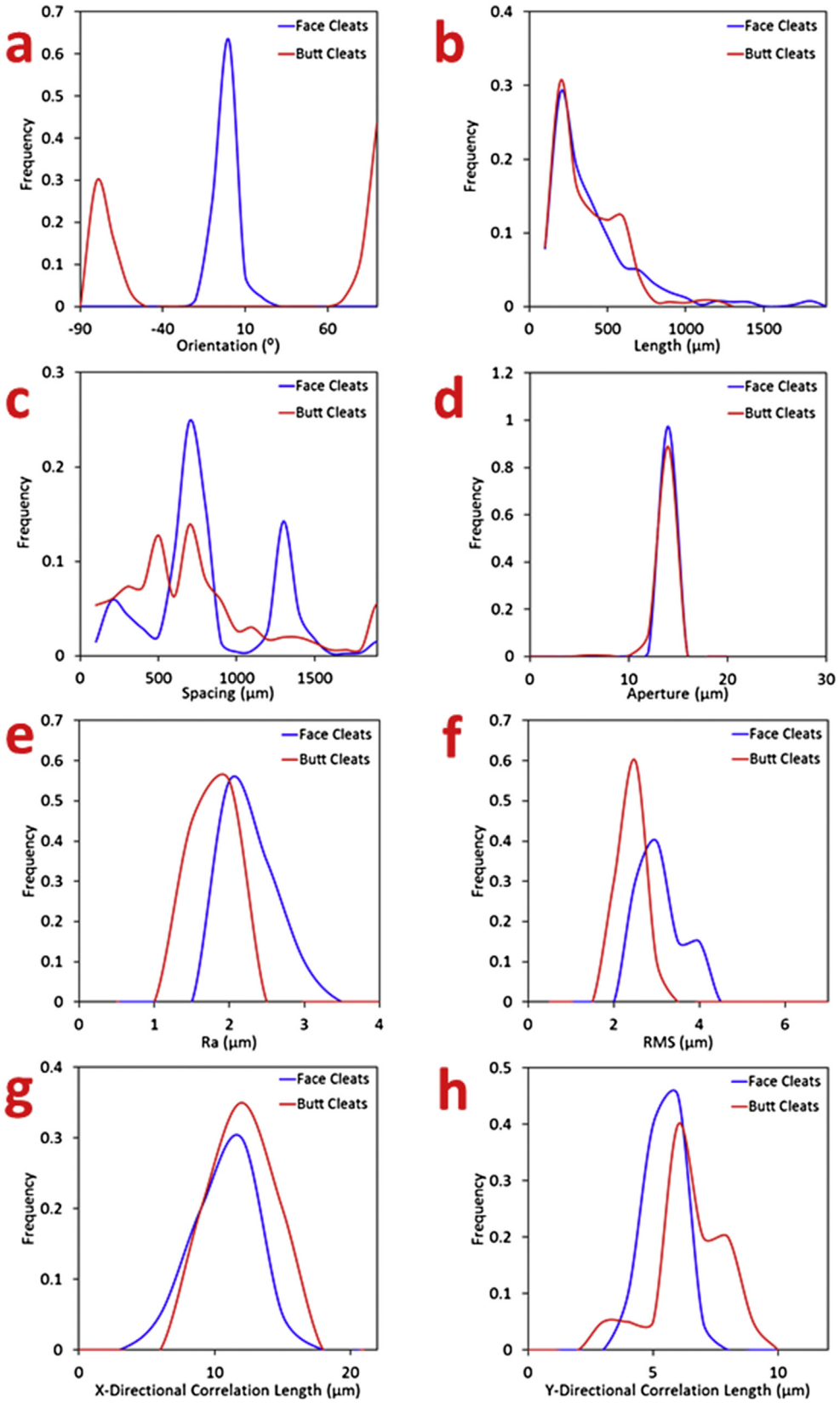

Fig. 9. Measured cleat statistics from micro-CT images: (a) orientation in XY plane, (b) length, (c) spacing, (d) aperture size and (e–h) roughness descriptors. Analysed roughness descriptors include (e) Ra (arithmetic mean absolute deviation), (f) RMS (root mean square deviation), and directional correlation lengths in X- and Y-directions (g–h), which measure how quickly a random surface decays.

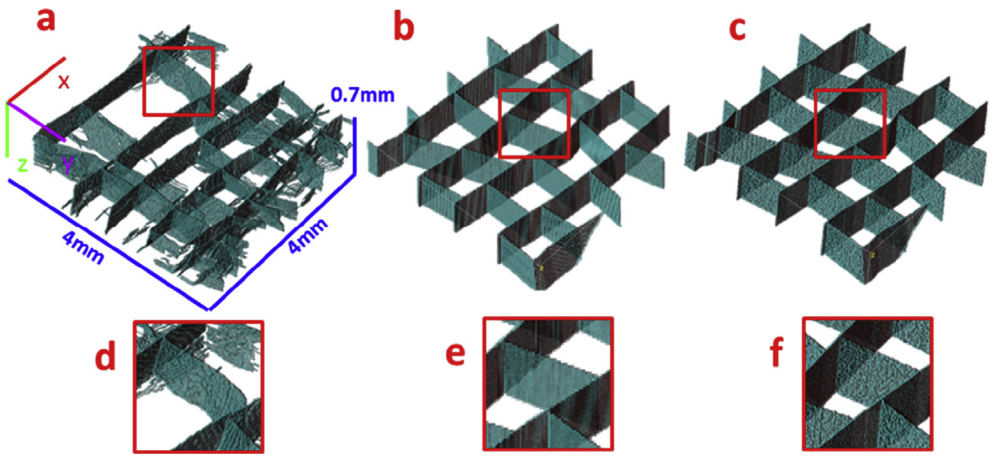

Fig. 10. (a) The schematic of original micro-CT image, (b) DFN and (c) rough-walled DFN models. The DFN model represents the main features of the original micro-CT image, e.g. the particular "T-junctions". It can be seen that the rough-walled DFN further preserves the local heterogeneity of the original image, by comparing the real cleat (d), reconstructed cleats with smooth surfaces (e) and rough surfaces (f). This approach is specifically important when the original image is noisy, poorly segmented, and/or has low resolution.

A schematic of chip fabrication is illustrated in Fig. 12. They conducted an experimental setup which mimics flow transport in CSG reservoirs. High-resolution microscope and camera were used to capture motion of water and gas displacement in this multiphase flow system. Water (non-wetting fluid) displaces gas (wetting fluid) in the fabricated coal cleat structure and follows the flow behaviour of a gas-wet system (Fig. 13). Complex transport in the coal cleat network was analysed by measuring the relative permeability of the microfluidic chip.

The increasing number of publications implementing microfluidic technique for studying multiphase flow transport emphasises on the potential of this method in explaining displacement mechanisms in porous media. Coal seams are considered to be one of the most essential and critical areas in which microfluidic approaches can provide important insights. Displacement processes in coal cleats are associated with unique mechanisms that are not completely understood and require further studies. This includes the change of contact angle, sorption on cleat surfaces and diffusion in the matrices. Another example is swelling and shrinkage of the coal matrix due to adsorption and desorption mechanisms, which affects coal permeability (Brochard et al., 2012; Mazumder and Wolf, 2008). The effects of reservoir temperature, solid matrix deformation and mechanical stress on flow characterisation also require further studies that could be directed toward microfluidics.

4.2. Contact angle measurements

Wettability, in addition to interfacial tension and capillary pressure, is known to control fluid distribution and behaviour in porous media. It is one of the most effective parameters for prediction of gas displacement and storage in reservoirs and controlling properties such as relative permeabilities and capillary pressure (Chiquet et al., 2007; Espinoza and Santamarina, 2010; Kaveh et al., 2011; Plug et al., 2008; Saghafi et al., 2014). Therefore, studying the wettability behaviour of coal can help to better understand pore-scale flow mechanisms. The assessment of wettability can improve the estimation of petrophysical properties, i.e. relative permeability and capillary pressure, in coal. Moreover, the observation of wetting behaviour in coal at the pore scale can show the dispersed phase and residual phase distributions. For design of representative microfluidic chips, accurate measurement of contact angles is also critical.

Wettability of reservoir rocks is determined through interfacial interactions between the rock and the reservoir fluids. Commonly, the contact angle is measured for evaluation of wettability in reservoirs. The Young (1805) equation is used to explain the equilibrium between three phases in contact (water, gas and rock) and to calculate the contact angle

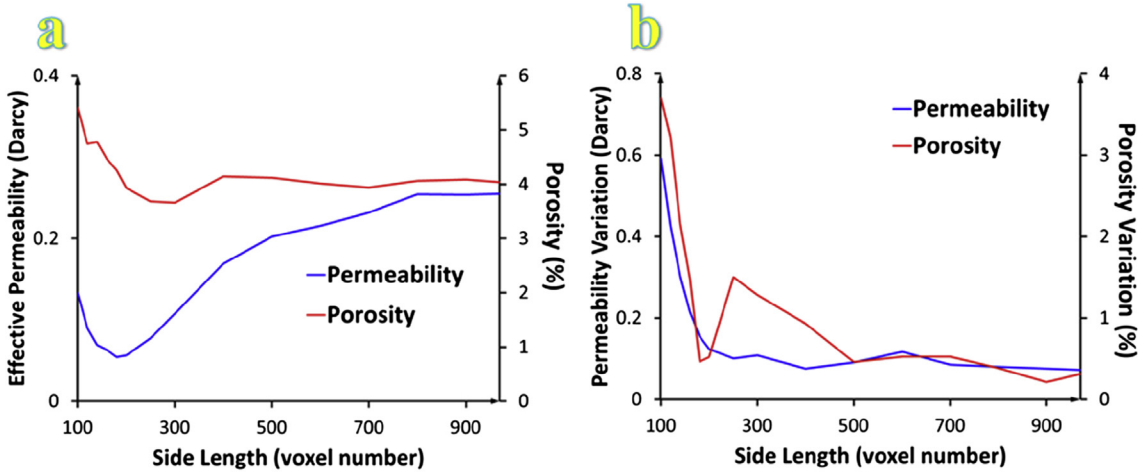

Fig. 11. (a) Average permeability and porosity values and (b) their variations with varying domain dimensions.

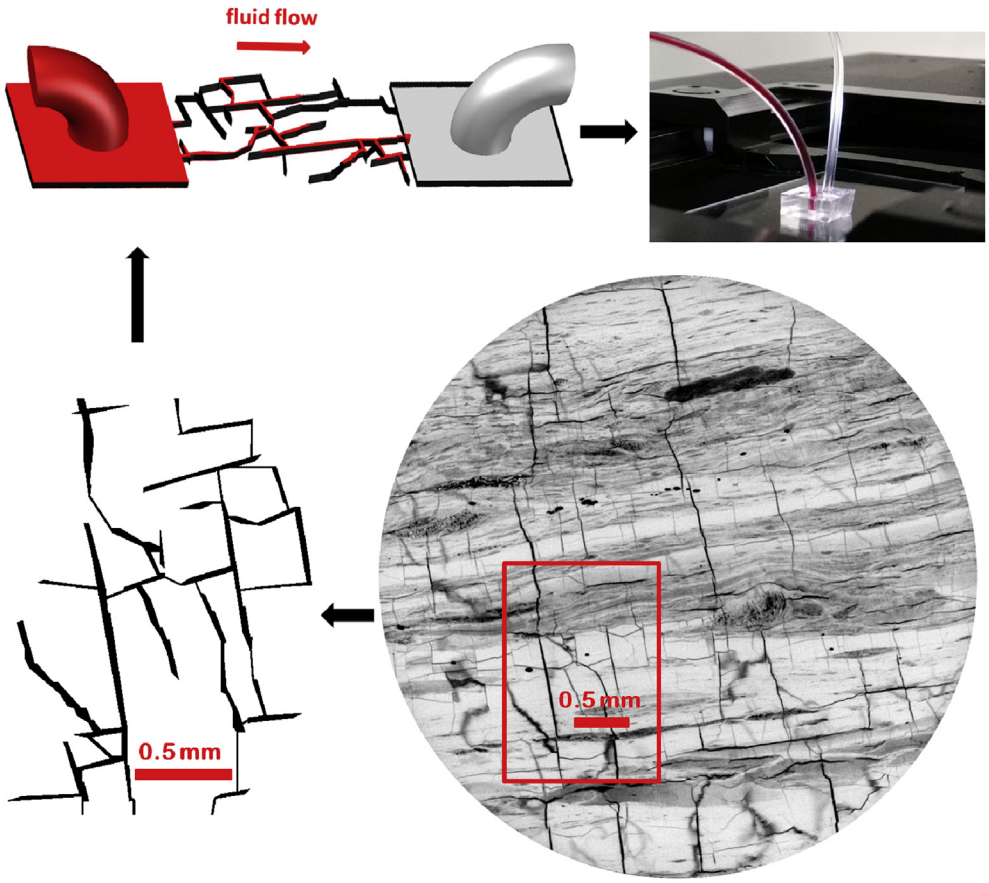

Fig. 12. Schematic workflow of microfluidic chip fabrication based on a real coal fracture structure. A region of interest is chosen from a coal micro-CT image. Then, PDMS chips are fabricated based on the structure and are used for flow experiments.

$$\gamma_{1g}\cos\theta = \gamma_{1s} - \gamma_{sg} \quad (3)$$

where θ is the contact angle, γ is the interfacial tension, and subscripts s, l and g represent solid, liquid and gas phases, respectively. The contact angle between the three phases (Fig. 14) determines whether the rock is gas wet ($\theta < 90^\circ$) or water wet ($\theta > 90^\circ$).

Limited studies have focused on the wettability characteristics of coal seams (Kaveh et al., 2011, 2012; Plug et al., 2008; Saghafi et al., 2014; Sakurovs and Lavrencic, 2011; Siemons et al., 2006). They have demonstrated the significant effect that reservoir pressure, temperature, and rank of coal can have on contact angle. Wettability alteration from water-wet to CO_2-wet has been reported at low pressure (approximately 0.27 MPa) and high pressure (approximately 8.7 MPa) for high- and medium-rank coals, respectively (Siemons et al., 2006). Plug et al. (2008) used capillary pressure between CO_2/water to investigate the wettability of the coal. They showed that the wettability of the medium-rank coal changes from water-wet to CO_2-wet with increasing system pressures whereas high-rank coal is CO_2-wet in all of the pressure range

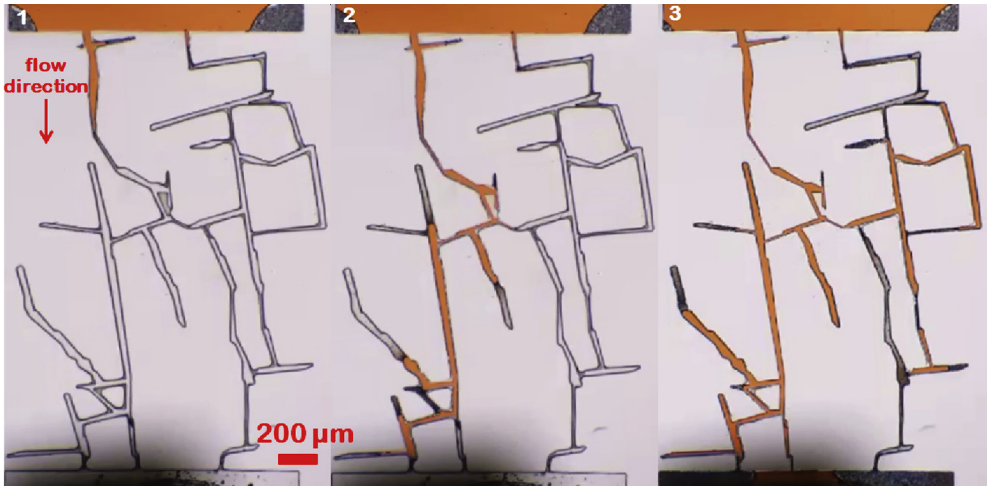

Fig. 13. Displacement of gas with water in a fabricated coal cleat structure (Gerami et al., 2016).

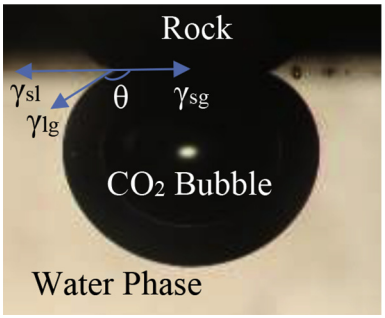

Fig. 14. A captive bubble of CO_2 on coal surface used for measuring contact angle.

tested. Sakurovs and Lavrencic (2011) showed high-rank coals are CO_2 wet at high pressures. Kaveh et al. (2011, 2012) discussed the tendency of high-rank coals to be gas wet in comparison with low-rank coals. Saghafi et al. (2014) compared the contact angle for different gases (CH_4, N_2 and CO_2) in a gas/water/coal system and reported the data at atmospheric temperature for a range of pressure values (1.8–15.3 MPa). They concluded a higher wettability of CO_2 relative to CH_4 and N_2 which explains high storage capacity of CO_2 in coal seam reservoirs.

We report an experiment on water/CO_2/coal system using the captive bubble method (Neumann and Good, 1979) to measure the contact angle at different pressures. The experiments are performed at 50°C and pressure was varied from 3 to 13 MPa. Our results are in agreements with the data reported by Saghafi et al. (2014) demonstrating the reduction in the contact angle by increasing the pressure, i.e. contact angle reduces 15% when changing pressure from 3Mpa to 13Mpa (Fig. 15). In coal, the contact angle cannot be assumed as a constant attribute as it may vary dynamically during the recovery processes. In addition, wettability affects the adsorption and desorption characteristics of gases in coal seams emphasising the need for reliable prediction of wettability in coals. A thorough understanding of coal surface chemistry and forces is required to explain the contact angle variations for different pressure and temperature conditions.

5. Discussion and challenges

5.1. Petrophysical analysis

Segmented micro-CT images can be used for calculations of important petrophysical properties of rocks (Arns et al., 2001, 2002; Knackstedt et al., 2004). For conventional rocks, the porosity can be calculated directly by finding the fraction of voxels that are labelled in the pore phase (Arns et al., 2005). However, in coal seams, a large

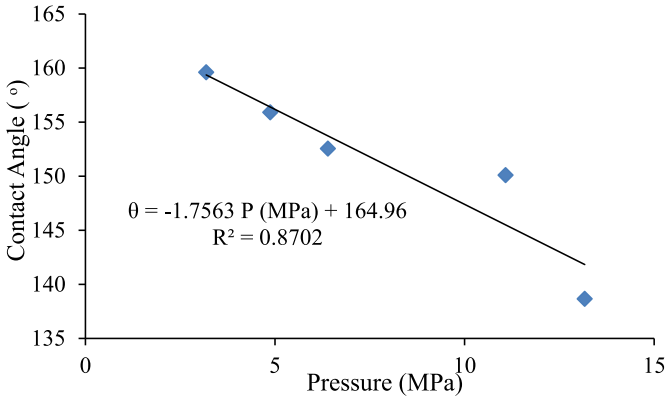

Fig. 15. Variation of CO_2 contact angle versus pressure on coal surface.

fraction of cleats are smaller than the resolution of the micro-CT scanner. This causes further complexity in porosity estimation of coals. Ramandi et al. (2016b) categorised porosity in coal micro-CT images into (i) resolved porosity and (ii) sub-resolution porosity and the summation of these two porosities provide the total porosity. The resolved porosity is simply calculated by the ratio of the number of voxels in the resolved porosity phase. To calculate the sub-resolution porosity from micro-CT data that includes porosity of sub-resolution pores and fractures, it is assumed that the solid phase of the sample is monomineralic. It can then be assumed that the grey-scale value of a voxel in the sub-resolution phase is linearly related to the sub-resolution porosity of that voxel. Two cut-off grey-scale values for 100% void and 100% solid are determined using the method explained in Ghous et al. (2007). For any voxel with grey-scale values between these two cut-off values, linear scale sub-resolution porosity is assigned. This scheme provides an accurate measurement of porosity where both resolved and sub-resolution porosity are included.

For calculation of absolute permeability on micro-CT images, commonly Stokes flow along with conservation of mass are solved numerically (Apourvari and Arns, 2015; Mostaghimi et al., 2013). Lattice Boltzmann methods are popular for simulation of flow and prediction of permeability of micro-CT images. The main challenge with coal micro-CT images is the distribution of cleat sizes such that aperture sizes may be captured by only 1–2 voxels. This causes numerical instability using lattice Boltzmann methods (Manwart et al., 2002). Another approach is estimating the permeability by obtaining a numerical solution for the Laplace's equation (Arns et al., 2003; Ramandi et al., 2016b). This method has shown to be computationally efficient and not limited in terms of number of voxels covering each flow pathways. There are approaches to circumvent these issues by usage of grid refinement techniques were data sets are up-sampled based on grey-scale micro-CT data and/or generation of representative cleat systems using DFN and Monte Carlo simulations.

Regardless of the technique employed to measure coal petrophysical properties and the need for further developments, we can already identify unique coal properties. Fig. 16 shows the results of simulations on several subsets of a coal micro-CT images using the explained methods for porosity and permeability. The results demonstrate two distinct clusters of values of permeability and no direct relationship between permeability and porosity in the tested coal. This is in contrast to conventional reservoir rocks where commonly permeability is correlated to porosity (Mostaghimi et al., 2013). This is perhaps because coal permeability mainly correlates to the fracture porosity (Chen et al., 2012, 2015; Gu, 2009; Palmer and Mansoori, 1996) rather than the total porosity, which is often observed for porous rock. Bright band coal often has high cleat density whereas the dull band contains low permeability microporosity with low cleat density.

Several attempts have been made for estimation of relative permeability of coals. This includes steady-state methods (Honarpour and Mahmood, 1988; Hyman et al., 1992; Nourbakhsh, 2012), unsteady-state methods (Christiansen et al., 1997; Johnson et al., 1959; Maloney and Doggett, 1995), history matching (Aminian et al., 2004; Meaney and Paterson, 1996; Young et al., 1991a, 1991b), capillary pressure methods (Nourbakhsh, 2012; Taber et al., 1974) and analysis of the production data (Clarkson et al., 2007, 2011; Fetkovich et al., 1986). This paper will not review the advantages and limitations of these methods and will not discuss the methods in detail. Rather the reader should reference the relative permeability review by Zhang et al. (2015). Even though a variety of experimental methods have been tested for obtaining relative permeability curves for coals, very limited investigations have been conducted for comparing the obtained relative

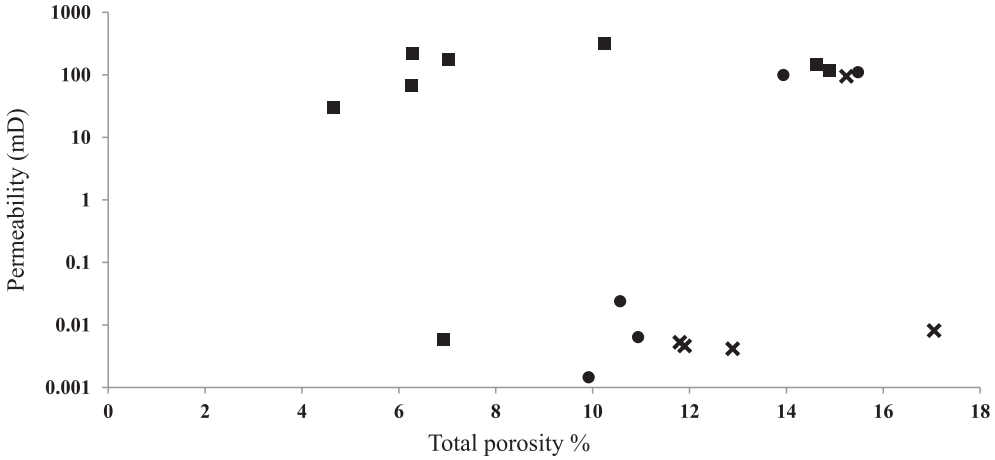

Fig. 16. Permeability estimation results. The logarithmic permeabilities of coal subsets plotted against their total porosities (squares: bright band, circles: intermediate and crosses: dull band). The high permeability cluster contains subsets with more bright bands while the low permeability cluster contains the subsets with more dull bands (Ramandi et al., 2016b).

permeability curves from different methods. In addition, pore-scale modelling for calculations of relative permeability curves in conventional rocks has been performed for more than a decade but it has not been translated to CSG industries (Blunt et al., 2002, 2013; Joekar-Niasar and Hassanizadeh, 2012; Raoof and Hassanizadeh, 2012). Combination of micro-CT imaging data and advanced numerical methods for calculation of multiphase flow in porous media can provide important insights to displacement of water and gas in coal seams. Lattice Boltzmann Methods (He et al., 1999; Shan and Chen, 1993), Smooth Particle Hydrodynamics (Tartakovsky and Meakin, 2005) and Volume of Fluid Methods (Raeini et al., 2012, 2014) have been tested for calculation of multiphase flow on micro-CT images and it is anticipated to test the applicability of these methods on coal samples. However, the main limitation is that cleats are planar in shape and are often only resolved by a few voxels in the direction normal to the cleat plane. For many numerical methods this will cause limitations without implementing grid refinement techniques.

Another simulation approach is a pore morphological method such as the capillary drainage transform (CDT) simulation, which is computationally efficient (Hilpert and Miller, 2001). This method belongs to the family of quasi-static methods where viscous effects are ignored. In this method, the Euclidean distance map (EDM) is first calculated directly from the pore geometry. Then, based on applying several thresholds on the EDM and connectivity checks, CDT maps are derived representing different distributions for the wetting and non-wetting phases at different pressure drops. Then, single phase flow simulations can be performed for each phase and the effective permeability for each phase is normalised by the absolute permeability to obtain the relative permeability. This method has shown to be capable of reproducing laboratory measurements of the drainage processes (Berg et al., 2016). However, this method also suffers from the lack of resolution obtained in the direction normal to the fracture plan when imaging a representative volume of coal. Fig. 17 shows the relative permeability points calculated using this method on the Moura coal (Ramandi et al., 2016b) and compared with the relative permeability values obtained from the literature for Australian coals (Chen et al., 2014). As demonstrated in Fig. 17, the CDT method provides only a limited number of data points for the relative permeability curve due to limited data resolution. Chen et al. (2013) proposed an improved relative permeability model accounting for porosity change due to stress variation or swelling/shrinkage effects. In the presented relative permeability curves, the swelling and shrinkage of coal matrix has been ignored. In other words, we assume the fracture properties and geometries do not change during displacement processes, and relative permeability is only affected by the invasion-percolation process. Therefore, this is another challenge that must be faced when simulating the flow properties of coal.

Overall the limitations associated with this approach are the limited number of saturation points, exclusion of viscous forces and the lack of control over the contact angle. The number of saturation points is dependent upon the pore morphology and the image resolution of the sample. In addition, the CDT approach assumes a fully water-wet surface while the coal is usually considered as a mixed-wet rock with variable contact angles (Saghafi et al., 2014). Future numerical modifications on pore morphological approaches could adapt these methods for more reliable calculations of relative permeability curves on micro-CT images.

5.2. Size versus resolution and REV

The natural fracture system in coals can span from micro to nanometres for endogenous fractures formed during coalification to hundreds of metres for exogenous fractures resulting from tectonic activities. The techniques for analyses and measurements for these fractures range from 2D visual observation of outcrops, high magnification microscopy to SEM and micro-CT imaging. With micro-CT imaging of coal, we face challenges with the trade-off between sample volume and image resolution. In the data presented in Figs. 1 and 2, we visualise cleat structure in a one-inch core at a resolution of 16 μm. However, coal samples have micro-porosity well below the image resolution, which is not well defined. We also observe large quasi-2D fractures that are thin in terms of image resolution. To accurately define the topology and in particular the connectivity of these systems, we require reasonably large core plugs, which results in limited fracture aperture resolution. In larger core plugs of 80 mm diameter, we also observe larger fractures but poorly resolve the micro-fissures and micro-porosity.

One possible solution is the incorporation of multiscale information from micro-porosity to interconnected larger scale cleat systems using statistical data from multi-resolution micro-CT and SEM data (Gerke et al., 2015; Ramandi et al., 2017; Tahmasebi et al., 2015). The conventional approaches of digital rock technology applied on conventional core samples where a single resolution image is collected will require modifications for CSG industries.

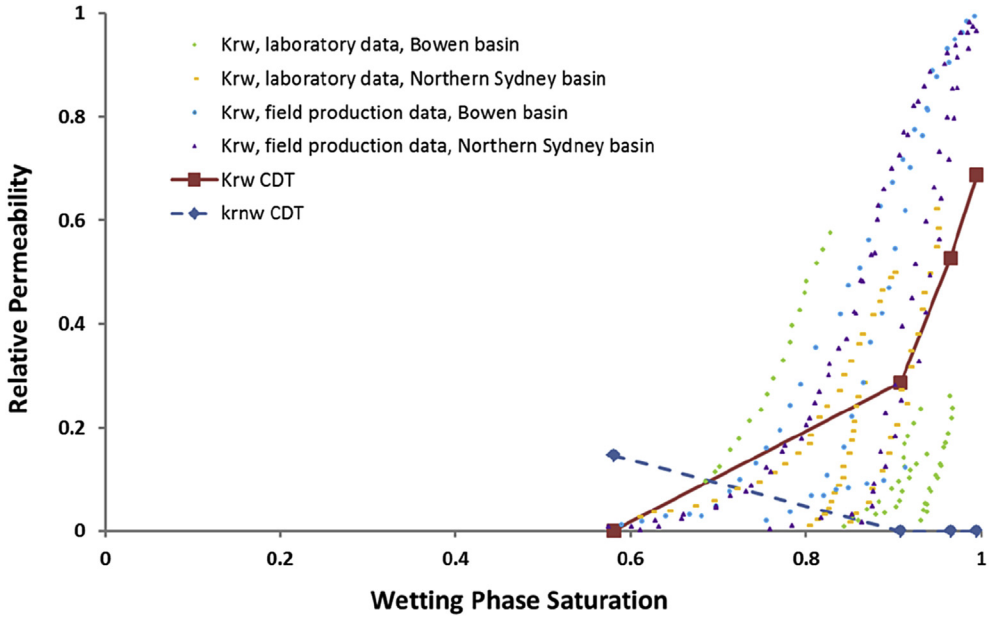

Fig. 17. Comparison of numerical relative permeability of the Moura coal and the relative permeability values obtained from the literature (Chen et al., 2014) for Australian coals. The solid and dashed lines are the wetting phase (water) and non-wetting phase (gas) relative permeability curves calculated numerically on the micro-CT image.

Sub-cleat scale information is required to model the complex multiphysics and thus petrophysical properties of coal. Jing et al. (2016) showed how the statistical information gathered from coal micro-CT images can be used for reconstruction of coal images that are not limited in terms of image resolution. Other approaches could utilise SEM data to present cleat roughness, which would affect cleat permeability and also larger scale CT images to characterise the multi-point statistic of cleat lithotypes and thus the spatial arrangements of bright and dull bands. There is need for thorough studies on the existence and size of a representative elementary volume (REV) for coal using multiscale imaging techniques.

5.3. Population into reservoir simulators

Reservoir simulation is the common practise for calculations of fluids displacement and prediction of recovery from hydrocarbon reservoirs (Aziz and Settari, 1979; Babaei and King, 2012; Bourbiaux, 2010; Bourbiaux et al., 2002; Hajibeygi et al., 2012; Jackson et al., 2013, 2015; Kumar et al., 2005; Li and Hao, 2006; Mostaghimi et al., 2015a; Mostaghimi et al., 2014, 2015b, 2016a; Mostaghimi and Mahani, 2010; Pan and Connell, 2009; Seidle and Arri, 1990; Shi et al., 2008; Su et al., 2015). For CSG reservoirs, the reservoir simulation is conducted for the prediction of gas production as well as estimation of efficiency of CO_2 injection into these formations for both storage and enhanced recovery (Karacan and Olea, 2015; Vishal et al., 2013). This paper has reviewed some of the practices to predict coal properties from the pore to core scales. However, coal is heterogeneous at multiscale and thus population of these data into a reservoir simulator for prediction of gas recovery is still a challenge. This requires integration of modelling tools and combining data obtained at different scales. The challenge of moving across scales has led to development of a range of upscaling methods (Blunt et al., 2013; King et al., 1998; Raoof et al., 2010; Rhodes et al., 2008) that should be translated to CSG applications. The other challenge is the coupling of molecular phenomena to Stokes and Darcy flow in the cleats. In addition, coal petrophysical properties including its porosity, permeability, relative permeability and contact angle are strongly dependent upon the reservoir pressure (Wei et al., 2007). This indicates that there is need for development of specific modules to accommodate these unique attributes in CSG reservoir simulations.

6. Conclusions

CSG reservoirs are an important resource for natural gas that are gaining increasing interest due to their environmental benefit and abundance. Understanding the displacement of gas and water in coal, which is controlled by the microscale cleat system is critical for explaining gas recovery processes. This paper has reviewed recent developments in cleat-scale characterisation of coal including (i) micro-CT imaging at wet and dry conditions; (ii) image enhancement and segmentation; (iii) developing methods for imaging diffusion processes in low-permeability structures; (iv) extraction of cleat statistics and reconstruction of the coal cleat system; and (v) developments of microfluidic methods for understanding and visualising immiscible displacement in the cleats and measurement of coal contact angle. These previous studies have visualised the underlying cleat structure of coal and provided information on the distribution of cleat properties. This is the first step for identifying coal types based on their pore-scale morphology and calculated cleat properties. The segmented micro-CT images have been used for calculation of coal petrophysical properties. The use of microfluidic methods can further improve our understanding of two-phase flow displacement in cleat geometries. However, microfluidic methods are limited to two-dimensional analyses.

We discussed challenges in the development of pore-scale imaging and modelling techniques for CSG applications. Computation of petrophysical properties from coal micro-CT images requires further calculations due to existence of micro-porosities and tiny pores and cleats causing numerical instability. Prediction of the relative permeability curves numerically requires developments of advanced numerical methods resolving the complex multiphase flow of water and gas in cleat systems. Pore morphological approaches can be an efficient candidate for thee simulations;

however, more work is anticipated to be conducted to adapt these approaches for CSG reservoirs. Another challenge is the limitation of the image size and resolution using micro-CT scanners. Accurate determination of cleat apertures requires high-resolution imaging leading to a smaller field of view. Developments of fusion imaging methods for CSG applications are recommended. Finally, multiscale data are required to be populated into reservoir simulators, which require integration of data and consistent representation of data into a reservoir model. This will be possible by enhanced computational facilities and developments of upscaling and downscaling methods. Furthermore, displacement of fluids in coal seams is a coupling between molecular phenomena with Darcy and Stokes flow, and the petrophysical properties are subject to change during the life of the reservoir. Thus, proper numerical methods must be designed to account for the multiphysics at the multiscale to provide reliable, efficient and accurate prediction of recovery from these reservoirs.

References

Aminian, K., Ameri, S., Bhavsar, A., Sanchez, M., Garcia, A., 2004. Type curves for coalbed methane production prediction. In: SPE Eastern Regional Meeting. Society of Petroleum Engineers.

Apourvari, S.N., Arns, C.H., 2015. Image-based relative permeability upscaling from the pore scale. Adv. Water Resour. 95, 161–175.

Armstrong, R.T., Georgiadis, A., Ott, H., Klemin, D., Berg, S., 2014. Critical capillary number: desaturation studied with fast X-ray computed microtomography. Geophys. Res. Lett. 41, 55–60.

Armstrong, R.T., McClure, J.E., Berrill, M.A., Rücker, M., Schlüter, S., Berg, S., 2016. Beyond Darcy's law: the role of phase topology and ganglion dynamics for two-fluid flow. Phys. Rev. E 94, 043113.

Arns, C.H., Bauget, F., Limaye, A., Sakellariou, A., Senden, T., Sheppard, A., Sok, R.M., Pinczewski, V., Bakke, S., Berge, L.I., 2005. Pore scale characterization of carbonates using X-ray microtomography. Spe J. 10, 475–484.

Arns, C.H., Knackstedt, M.A., Pinczewski, M.V., Lindquist, W., 2001. Accurate estimation of transport properties from microtomographic images. Geophys. Res. Lett. 28, 3361–3364.

Arns, C.H., Knackstedt, M.A., Pinczewski, W.V., Garboczi, E.J., 2002. Computation of linear elastic properties from microtomographic images: methodology and agreement between theory and experiment. Geophysics 67, 1396–1405.

Arns, J.-Y., Arns, C.H., Sheppard, A.P., Sok, R.M., Knackstedt, M.A., Pinczewski, W.V., 2003. Relative permeability from tomographic images; effect of correlated heterogeneity. J. Pet. Sci. Eng. 39, 247–259.

Avraam, D., Payatakes, A., 1999. Flow mechanisms, relative permeabilities, and coupling effects in steady-state two-phase flow through porous media. The case of strong wettability. Ind. Eng. Chem. Res. 38, 778–786.

Aziz, K., Settari, A., 1979. Petroleum Reservoir Simulation. Chapman & Hall.

Babaei, M., King, P.R., 2012. A modified nested-gridding for upscaling–downscaling in reservoir simulation. Transp. Porous Media 93, 753–775.

Baecher, G., Lanney, N., Einstein, H., 1977. Statistical description of rock properties and sampling. In: The 18th US Symposium on Rock Mechanics (USRMS). American Rock Mechanics Association.

Berg, S., Rücker, M., Ott, H., Georgiadis, A., van der Linde, H., Enzmann, F., Kersten, M., Armstrong, R., de With, S., Becker, J., 2016. Connected pathway relative permeability from pore-scale imaging of imbibition. Adv. Water Resour. 90, 24–35.

Bigun, J., Bigun, T., Nilsson, K., 2004. Recognition by symmetry derivatives and the generalized structure tensor. IEEE Trans. Pattern Anal. Mach. Intell. 26, 1590–1605.

Bijeljic, B., Blunt, M.J., 2006. Pore-scale modeling and continuous time random walk analysis of dispersion in porous media. Water Resour. Res. 42.

Bijeljic, B., Mostaghimi, P., Blunt, M.J., 2011. Signature of non-Fickian solute transport in complex heterogeneous porous media. Phys. Rev. Lett. 107, 204502.

Blunt, M.J., 2001. Flow in porous media—pore-network models and multiphase flow. Curr. Opin. Colloid & Interface Sci. 6, 197–207.

Blunt, M.J., Bijeljic, B., Dong, H., Gharbi, O., Iglauer, S., Mostaghimi, P., Paluszny, A., Pentland, C., 2013. Pore-scale imaging and modelling. Adv. Water Resour. 51, 197–216.

Blunt, M.J., Jackson, M.D., Piri, M., Valvatne, P.H., 2002. Detailed physics, predictive capabilities and macroscopic consequences for pore-network models of multiphase flow. Adv. Water Resour. 25, 1069–1089.

Bossie-Codreanu, D., Wolf, K.-H.A., Ephraim, R., 2004. A new characterization method for coal bed methane. Geol. Belg. 7, 37–145.

Bourbiaux, B., 2010. Fractured reservoir simulation: a challenging and rewarding issue. Oil Gas Sci. Technol.–Revue de l'Institut Français du Pétrole 65, 227–238.

Bourbiaux, B., Basquet, R., Cacas, M.-C., Daniel, J.-M., Sarda, S., 2002. An integrated workflow to account for multi-scale fractures in reservoir simulation models: implementation and benefits. In: Abu Dhabi International Petroleum Exhibition and Conference. Society of Petroleum Engineers.

Brochard, L., Vandamme, M., Pellenq, R.J.-M., Fen-Chong, T., 2012. Adsorption-induced deformation of microporous materials: coal swelling induced by CO2–CH4 competitive adsorption. Langmuir 28, 2659–2670.

Cacas, M., Ledoux, E., Marsily, G.d., Barbreau, A., Calmels, P., Gaillard, B., Margritta, R., 1990. Modeling fracture flow with a stochastic discrete fracture network: calibration and validation: 2. The transport model. Water Resour. Res. 26, 491–500.

Cai, Y., Liu, D., Mathews, J.P., Pan, Z., Elsworth, D., Yao, Y., Li, J., Guo, X., 2014. Permeability evolution in fractured coal—combining triaxial confinement with X-ray computed tomography, acoustic emission and ultrasonic techniques. Int. J. Coal Geol. 122, 91–104.

Catmull, E., Rom, R., 1974. A class of local interpolating splines. Comput. Aided Geom. Des. 74, 317–326.

Cavé, L., Al, T., Xiang, Y., Vilks, P., 2009. A technique for estimating one-dimensional diffusion coefficients in low-permeability sedimentary rock using X-ray radiography: comparison with through-diffusion measurements. J. Contam. Hydrol. 103, 1–12.

Chen, D., Pan, Z., Liu, J., Connell, L.D., 2012. Characteristic of anisotropic coal permeability and its impact on optimal design of multi-lateral well for coalbed methane production. J. Pet. Sci. Eng. 88, 13–28.

Chen, D., Pan, Z., Liu, J., Connell, L.D., 2013. An improved relative permeability model for coal reservoirs. Int. J. Coal Geol. 109, 45–57.

Chen, D., Pan, Z., Ye, Z., 2015. Dependence of gas shale fracture permeability on effective stress and reservoir pressure: model match and insights. Fuel 139, 383–392.

Chen, D., Shi, J.-Q., Durucan, S., Korre, A., 2014. Gas and water relative permeability in different coals: model match and new insights. Int. J. Coal Geol. 122, 37–49.

Chen, S.H., Feng, X.M., Isam, S., 2008. Numerical estimation of REV and permeability tensor for fractured rock masses by composite element method. Int. J. Numer. Anal. Methods Geomechanics 32, 1459–1477.

Chiquet, P., Broseta, D., Thibeau, S., 2007. Wettability alteration of caprock minerals by carbon dioxide. Geofluids 7, 112–122.

Christiansen, R.L., Kalbus, J.S., Howarth, S.M., 1997. Evaluation of Methods for Measuring Relative Permeability of Anhydride from the Salado Formation: Sensitivity Analysis and Data Reduction. Sandia National Labs, Albuquerque, NM (United States).

Clarkson, C., Bustin, R., 1999. The effect of pore structure and gas pressure upon the transport properties of coal: a laboratory and modeling study. 1. Isotherms and pore volume distributions. Fuel 78, 1333–1344.

Clarkson, C.R., Jordan, C.L., Gierhart, R.R., Seidle, J.P., 2007. Production data analysis of CBM wells. In: Rocky Mountain Oil & Gas Technology Symposium. Society of Petroleum Engineers.

Clarkson, C.R., Rahmanian, M., Kantzas, A., Morad, K., 2011. Relative permeability of CBM reservoirs: controls on curve shape. Int. J. Coal Geol. 88, 204–217.

Cossé, R., 1993. Basics of Reservoir Engineering: Oil and Gas Field Development Techniques. Éditions Technip.

De Kock, T., Boone, M.A., De Schryver, T., Van Stappen, J., Derluyn, H., Masschaele, B., De Schutter, G., Cnudde, V., 2015. A pore-scale study of fracture dynamics in rock using X-ray micro-CT under ambient freeze–thaw cycling. Environ. Sci. Technol. 49, 2867–2874.

Deisman, N., Ivars, D.M., Darcel, C., Chalaturnyk, R.J., 2010. Empirical and numerical approaches for geomechanical characterization of coal seam reservoirs. Int. J. Coal Geol. 82, 204–212.

Espinoza, D.N., Santamarina, J.C., 2010. Water-CO2-mineral systems: interfacial tension, contact angle, and diffusion—implications to CO2 geological storage. Water Resour. Res. 46.

Espinoza, D.N., Shovkun, I., Makni, O., Lenoir, N., 2016. Natural and induced fractures in coal cores imaged through X-ray computed microtomography—impact on desorption time. Int. J. Coal Geol. 154, 165–175.

Feng, Z., Zhou, D., Zhao, Y., Cai, T., 2016. Study on microstructural changes of coal after methane adsorption. J. Nat. Gas Sci. Eng. 30, 28–37.

Fetkovich, M., Guerrero, E., Fetkovich, M., Thomas, L., 1986. Oil and gas relative permeabilities determined from rate-time performance data. In: SPE Annual Technical Conference and Exhibition. Society of Petroleum Engineers.

Flores, R.M., 1998. Coalbed methane: from hazard to resource. Int. J. Coal Geol. 35, 3–26.

Fogden, A., Goergen, E., Olson, T., Cheng, Q., Middleton, J., Kingston, A., Curtis, M., Jernigen, J., 2015. Applications of multi-scale imaging techniques to unconventional reservoirs. In: SPE Asia Pacific Unconventional Resources Conference and Exhibition. Society of Petroleum Engineers.

Gale, J., Freund, P., 2001. Coal-Bed methane enhancement with CO2 sequestration worldwide potential. Environ. Geosci. 8, 210–217.

Gao, F., Stead, D., Kang, H., 2014. Numerical investigation of the scale effect and anisotropy in the strength and deformability of coal. Int. J. Coal Geol. 136, 25–37.

Gash, B.W., Volz, R.F., Potter, G., Corgan, J.M., 1992. The Effects of Cleat Orientation and Confining Pressure on Cleat Porosity, Permeability and Relative Permeability in Coal. paper 9321, pp. 17–21.

Gerami, A., Mostaghimi, P., Armstrong, R.T., Zamani, A., Warkiani, M.E., 2016. A microfluidic framework for studying relative permeability in coal. Int. J. Coal Geol. 159, 183–193.

Gerke, K.M., Karsanina, M.V., Mallants, D., 2015. Universal stochastic multiscale image fusion: an example application for shale rock. Sci. Rep. 5.

Ghous, A., Senden, T.J., Sok, R.M., Sheppard, A.P., Pinczewski, V.W., Knackstedt, M.A., 2007. 3D characterisation of microporosity in carbonate cores. In: SPWLA

Middle East Regional Symposium. Society of Petrophysicists and Well-Log Analysts.
Golab, A., Ward, C.R., Permana, A., Lennox, P., Botha, P., 2013. High-resolution three-dimensional imaging of coal using microfocus X-ray computed tomography, with special reference to modes of mineral occurrence. Int. J. Coal Geol. 113, 97–108.
Golab, A.N., Knackstedt, M.A., Averdunk, H., Senden, T., Butcher, A.R., Jaime, P., 2010. 3D porosity and mineralogy characterization in tight gas sandstones. Lead. Edge 29, 1476–1483.
Gray, I., 1987. Reservoir Engineering in Coal Seams: Part 1-The Physical Process of Gas Storage and Movement in Coal Seams.
Gu, F., 2009. Reservoir and Geomechanical Coupled Simulation of CO2 Sequestration and Enhanced Coalbed Methane Recovery. University of Alberta.
Guerrero Aconcha, U.E., Kantzas, A., 2009. Diffusion of hydrocarbon gases in heavy oil and bitumen. In: Latin American and Caribbean Petroleum Engineering Conference. Society of Petroleum Engineers.
Gunda, N.S.K., Bera, B., Karadimitriou, N.K., Mitra, S.K., Hassanizadeh, S.M., 2011. Reservoir-on-a-Chip (ROC): a new paradigm in reservoir engineering. Lab a Chip 11, 3785–3792.
Gunter, W.D., Gentzis, T., Rottenfusser, B.A., Richardson, R.J.H., 1997. Deep coalbed methane in Alberta, Canada: a fuel resource with the potential of zero greenhouse gas emissions. Energy Convers. Manag. 38 (Suppl.), S217–S222.
Hajibeygi, H., Lee, S.H., Lunati, I., 2012. Accurate and efficient simulation of multiphase flow in a heterogeneous reservoir with error estimate and control in the multiscale finite-volume framework. SPE J. 17, 1,071–071,083.
He, M., Wang, C., Feng, J., Li, D., Zhang, G., 2010. Experimental investigations on gas desorption and transport in stressed coal under isothermal conditions. Int. J. Coal Geol. 83, 377–386.
He, X., Chen, S., Zhang, R., 1999. A lattice Boltzmann scheme for incompressible multiphase flow and its application in simulation of Rayleigh–Taylor instability. J. Comput. Phys. 152, 642–663.
Heriawan, M.N., Koike, K., 2015. Coal quality related to microfractures identified by CT image analysis. Int. J. Coal Geol. 140, 97–110.
Hilpert, M., Miller, C.T., 2001. Pore-morphology-based simulation of drainage in totally wetting porous media. Adv. Water Resour. 24, 243–255.
Honarpour, M., Mahmood, S., 1988. Relative-permeability measurements: an overview. J. Pet. Technol. 40, 963–966.
Hsieh, J., 2009. Computed Tomography: Principles, Design, Artifacts, and Recent Advances. SPIE, Bellingham, WA.
Hyman, L., Brugler, M., Daneshjou, D., Ohen, H., 1992. Advances in laboratory measurement techniques of relative permeability and capillary pressure for coal seams. Q. Rev. Methane Coal Seams Technol. 9, 9–13.
Jackson, M., Gomes, J., Mostaghimi, P., Percival, J., Tollit, B., Pavlidis, D., Pain, C., El-Sheikh, A., Muggeridge, A., Blunt, M., 2013. Reservoir modeling for flow simulation using surfaces, adaptive unstructured meshes, and control-volume-finite-element methods. In: SPE Reservoir Simulation Symposium. Society of Petroleum Engineers.
Jackson, M., Percival, J., Mostaghimi, P., Tollit, B., Pavlidis, D., Pain, C., Gomes, J., Elsheikh, A.H., Salinas, P., Muggeridge, A., 2015. Reservoir modeling for flow simulation by use of surfaces, adaptive unstructured meshes, and an overlapping-control-volume finite-element method. SPE Reserv. Eval. Eng. 18, 115–132.
Jahne, B., 1993. Spatio-temporal Image Processing: Theory and Scientific Applications. Springer-Verlag New York, Inc.
Jing, Y., Armstrong, R.T., Mostaghimi, P., 2017. Rough-walled discrete fracture network modelling for coal characterisation. Fuel 191, 442–453.
Jing, Y., Armstrong, R.T., Ramandi, H.L., Mostaghimi, P., 2016. Coal cleat reconstruction using micro-computed tomography imaging. Fuel 181, 286–299.
Joekar-Niasar, V., Hassanizadeh, S., 2012. Analysis of fundamentals of two-phase flow in porous media using dynamic pore-network models: a review. Crit. Rev. Environ. Sci. Technol. 42, 1895–1976.
Johns, R.A., Steude, J.S., Castanier, L.M., Roberts, P.V., 1993. Nondestructive measurements of fracture aperture in crystalline rock cores using X ray computed tomography. J. Geophys. Res. Solid Earth 98, 1889–1900.
Johnson, E., Bossler, D., Bossler, V., 1959. Calculation of Relative Permeability from Displacement Experiments.
Joseph, J., Gunda, N.S.K., Mitra, S.K., 2013. On-chip porous media: porosity and permeability measurements. Chem. Eng. Sci. 99, 274–283.
Karacan, C., Okandan, E., 2001. Adsorption and gas transport in coal microstructure: investigation and evaluation by quantitative X-ray CT imaging. Fuel 80, 509–520.
Karacan, C.Ö., 2003. Heterogeneous sorption and swelling in a confined and stressed coal during CO2 injection. Energy & Fuels 17, 1595–1608.
Karacan, C.Ö., 2007. Swelling-induced volumetric strains internal to a stressed coal associated with CO 2 sorption. Int. J. Coal Geol. 72, 209–220.
Karacan, C.Ö., Mitchell, G.D., 2003. Behavior and effect of different coal microlithotypes during gas transport for carbon dioxide sequestration into coal seams. Int. J. Coal Geol. 53, 201–217.
Karacan, C.Ö., Olea, R.A., 2015. Stochastic reservoir simulation for the modeling of uncertainty in coal seam degasification. Fuel 148, 87–97.
Kaveh, N.S., Rudolph, E.S.J., Wolf, K.-H.A., Ashrafizadeh, S.N., 2011. Wettability determination by contact angle measurements: hvBb coal–water system with injection of synthetic flue gas and CO 2. J. Colloid Interface Sci. 364, 237–247.
Kaveh, N.S., Wolf, K., Ashrafizadeh, S., Rudolph, E., 2012. Effect of coal petrology and pressure on wetting properties of wet coal for CO 2 and flue gas storage. Int. J. Greenh. Gas Control 11, S91–S101.
Ketcham, R.A., Carlson, W.D., 2001. Acquisition, optimization and interpretation of X-ray computed tomographic imagery: applications to the geosciences. Comput. Geosciences 27, 381–400.
Ketcham, R.A., Slottke, D.T., Sharp, J.M., 2010. Three-dimensional measurement of fractures in heterogeneous materials using high-resolution X-ray computed tomography. Geosphere 6, 499–514.
King, G.R., Ertekin, T., Schwerer, F.C., 1986. Numerical simulation of the transient behavior of coal-seam degasification wells. SPE Form. Eval. 1, 165–183.
King, M., MacDonald, D., Todd, S., Leung, H., 1998. Application of novel upscaling approaches to the Magnus and Andrew reservoirs. In: European Petroleum Conference. Society of Petroleum Engineers.
Knackstedt, M., Arns, C., Limaye, A., Sakellariou, A., Senden, T., Sheppard, A., Sok, R., Pinczewski, W.V., Bunn, G., 2004. Digital Core Laboratory: properties of reservoir core derived from 3D images. In: SPE Asia Pacific Conference on Integrated Modelling for Asset Management. Society of Petroleum Engineers.
Kotarba, M.J., 2001. Composition and origin of coalbed gases in the Upper Silesian and Lublin basins, Poland. Org. Geochem. 32, 163–180.
Kumar, A., Noh, M.H., Ozah, R.C., Pope, G.A., Bryant, S.L., Sepehrnoori, K., Lake, L.W., 2005. Reservoir simulation of CO 2 storage in aquifers. Spe J. 10, 336–348.
Latham, S., Varslot, T., Sheppard, A., 2008. Image registration: enhancing and calibrating X-ray micro-CT imaging. In: Proc. of the Soc. Core Analysts (Abu Dhabi, UAE).
Laubach, S., Marrett, R., Olson, J., Scott, A., 1998. Characteristics and origins of coal cleat: a review. Int. J. Coal Geol. 35, 175–207.
Lee, T.-C., Kashyap, R.L., Chu, C.-N., 1994. Building skeleton models via 3-D medial surface axis thinning algorithms. CVGIP Graph. Models Image Process. 56, 462–478.
Li, J., Hao, T.-y., 2006. Review on methods of oil & gas reservoir stochastic simulation. Prog. Geophys. 2, 017.
Li, S., Tang, D., Xu, H., Yang, Z., 2012. Advanced characterization of physical properties of coals with different coal structures by nuclear magnetic resonance and X-ray computed tomography. Comput. Geosciences 48, 220–227.
Liu, M., Mostaghimi, P., 2017. High-resolution pore-scale simulation of dissolution in porous media. Chem. Eng. Sci. 161, 360–369.
Liu, S., Sang, S., Wang, G., Ma, J., Wang, X., Wang, W., Du, Y., Wang, T., 2017. FIB-SEM and X-ray CT characterization of interconnected pores in high-rank coal formed from regional metamorphism. J. Pet. Sci. Eng. 148, 21–31.
Liu, Y., Teng, Y., Lu, G., Jiang, L., Zhao, J., Zhang, Y., Song, Y., 2016. Experimental study on CO 2 diffusion in bulk n-decane and n-decane saturated porous media using micro-CT. Fluid Phase Equilibria 417, 212–219.
Lorig, L., Darcel, C., Damjanac, B., Pierce, M., Billaux, D., 2015. Application of discrete fracture networks in mining and civil geomechanics. Min. Technol. 124, 239–254.
Mahoney, S.A., Rufford, T.E., Dmyterko, A.S., Rudolph, V., Steel, K.M., 2015a. The effect of rank and lithotype on coal wettability and its application to coal relative permeability models. In: SPE Asia Pacific Unconventional Resources Conference and Exhibition. Society of Petroleum Engineers.
Mahoney, S.A., Rufford, T.E., Rudolph, V., Liu, K.-Y., Rodrigues, S., Steel, K.M., 2015b. Creation of microchannels in Bowen Basin coals using UV laser and reactive ion etching. Int. J. Coal Geol. 144, 48–57.
Maillot, J., Davy, P., De Dreuzy, J.-R., Le Goc, R., Darcel, C., Stigsson, M., 2014. Comparison between “Poissonian” and “mechanically-oriented” DFN models for the prediction of permeability and flow channeling. In: Proceedings of the First International Conference on Discrete Fracture Network Engineering (Vancouver).
Maloney, D., Doggett, K., 1995. Advances in Steady-and Unsteady-state Relative, Permeability Measurements and Correlations FY1995.
Manwart, C., Aaltosalmi, U., Koponen, A., Hilfer, R., Timonen, J., 2002. Lattice-Boltzmann and finite-difference simulations for the permeability for three-dimensional porous media. Phys. Rev. E 66, 016702.
Mao, L., Hao, N., An, L., Chiang, F.-p., Liu, H., 2015. 3D mapping of carbon dioxide-induced strain in coal using digital volumetric speckle photography technique and X-ray computer tomography. Int. J. Coal Geol. 147, 115–125.
Mathews, J.P., Pone, J.D.N., Mitchell, G.D., Halleck, P., 2011. High-resolution X-ray computed tomography observations of the thermal drying of lump-sized subbituminous coal. Fuel Process. Technol. 92, 58–64.
Mayo, S., Josh, M., Nesterets, Y., Esteban, L., Pervukhina, M., Clennell, M.B., Maksimenko, A., Hall, C., 2015. Quantitative micro-porosity characterization using synchrotron micro-CT and xenon K-edge subtraction in sandstones, carbonates, shales and coal. Fuel 154, 167–173.
Mazumder, S., Wolf, K.-H., Elewaut, K., Ephraim, R., 2006. Application of X-ray computed tomography for analyzing cleat spacing and cleat aperture in coal samples. Int. J. Coal Geol. 68, 205–222.
Mazumder, S., Wolf, K.H., 2008. Differential swelling and permeability change of coal in response to CO 2 injection for ECBM. Int. J. Coal Geol. 74, 123–138.
Meaney, K., Paterson, L., 1996. Relative permeability in coal. In: SPE Asia Pacific Oil and Gas Conference. Society of Petroleum Engineers.
Meng, Y., Tang, D., Xu, H., Qu, Y., Li, Y., Zhang, W., 2014. Division of coalbed methane desorption stages and its significance. Pet. Explor. Dev. 41, 671–677.
Menke, H.P., Bijeljic, B., Andrew, M.G., Blunt, M.J., 2015. Dynamic three-dimensional pore-scale imaging of reaction in a carbonate at reservoir conditions. Environ. Sci. Technol. 49, 4407–4414.
Montemagno, C., Pyrak-Nolte, L., 1999. Fracture network versus single fractures: measurement of fracture geometry with X-ray tomography. Phys. Chem. Earth,

Part A Solid Earth Geodesy 24, 575–579.
Moore, T.A., 2012. Coalbed methane: a review. Int. J. Coal Geol. 101, 36–81.
Mostaghimi, P., Armstrong, R.T., Gerami, A., Warkaini, M.E., Ramandi, H.L., Pinczewski, V., 2015a. Micro-CT imaging and microfluidics for understanding flow in coal seam reservoirs. In: Proc. of International Symposium of the Society of Core Analysts (Newfoundland, Canada).
Mostaghimi, P., Bijeljic, B., Blunt, M., 2012. Simulation of flow and dispersion on pore-space images. SPE J. 17, 1,131–131,141.
Mostaghimi, P., Blunt, M.J., Bijeljic, B., 2013. Computations of absolute permeability on micro-CT images. Math. Geosci. 45, 103–125.
Mostaghimi, P., Kamali, F., Jackson, M.D., Muggeridge, A.H., Pain, C.C., 2016a. Adaptive mesh optimization for simulation of immiscible viscous fingering. SPE J. 21, 2250–2259.
Mostaghimi, P., Liu, M., Arns, C.H., 2016b. Numerical simulation of reactive transport on micro-CT images. Math. Geosci. 48, 963–983.
Mostaghimi, P., Mahani, H., 2010. A quantitative and qualitative comparison of coarse-grid-generation techniques for modeling fluid displacement in heterogeneous porous media. SPE Reserv. Eval. Eng. 13, 24–36.
Mostaghimi, P., Percival, J.R., Pavlidis, D., Ferrier, R.J., Gomes, J.L., Gorman, G.J., Jackson, M.D., Neethling, S.J., Pain, C.C., 2015b. Anisotropic mesh adaptivity and control volume finite element methods for numerical simulation of multiphase flow in porous media. Math. Geosci. 47, 417–440.
Mostaghimi, P., Tollit, B.S., Neethling, S.J., Gorman, G.J., Pain, C.C., 2014. A control volume finite element method for adaptive mesh simulation of flow in heap leaching. J. Eng. Math. 87, 111–121.
Narasimhan, K.S., Mukherjee, A.K., Sengupta, S., Singh, S.M., Alam, M.M., 1998. Coal bed methane potential in India. Fuel 77, 1865–1866.
Naudé, G., Hoffman, J., Theron, S.J., Coetzer, G., 2013. The use of X-ray computed tomography in the characterisation of coal and associated char reductants. Miner. Eng. 52, 143–154.
Neumann, A.W., Good, R.J., 1979. Techniques of measuring contact angles. Surf. and Colloid Sci. 11, 31–91.
Nourbakhsh, A., 2012. Determination of Capillary Pressure, Relative Permeability and Pores Size Distribution Characteristics of Coal from Sydney Basin-Canada.
Palmer, I., Mansoori, J., 1996. How permeability depends on stress and pore pressure in coalbeds: a new model. In: SPE Annual Technical Conference and Exhibition. Society of Petroleum Engineers.
Pan, Z., Connell, L.D., 2009. Comparison of adsorption models in reservoir simulation of enhanced coalbed methane recovery and CO 2 sequestration in coal. Int. J. Greenh. Gas Control 3, 77–89.
Pan, Z., Connell, L.D., 2012. Modelling permeability for coal reservoirs: a review of analytical models and testing data. Int. J. Coal Geol. 92, 1–44.
Pan, Z., Connell, L.D., Camilleri, M., Connelly, L., 2010. Effects of matrix moisture on gas diffusion and flow in coal. Fuel 89, 3207–3217.
Pant, L.M., Huang, H., Secanell, M., Larter, S., Mitra, S.K., 2015. Multi scale characterization of coal structure for mass transport. Fuel 159, 315–323.
Peyton, R., Haeffner, B., Anderson, S., Gantzer, C., 1992. Applying X-ray CT to measure macropore diameters in undisturbed soil cores. Geoderma 53, 329–340.
Pillalamarry, M., Harpalani, S., Liu, S., 2011. Gas diffusion behavior of coal and its impact on production from coalbed methane reservoirs. Int. J. Coal Geol. 86, 342–348.
Plug, W.-J., Mazumder, S., Bruining, J., 2008. Capillary Pressure and Wettability Behavior of CO2 Sequestration in Coal at Elevated Pressures.
Polak, A., Grader, A.S., Wallach, R., Nativ, R., 2003. Tracer diffusion from a horizontal fracture into the surrounding matrix: measurement by computed tomography. J. Contam. Hydrol. 67, 95–112.
Pone, J.D.N., Halleck, P.M., Mathews, J.P., 2010. 3D characterization of coal strains induced by compression, carbon dioxide sorption, and desorption at in-situ stress conditions. Int. J. Coal Geol. 82, 262–268.
Pone, J.D.N., Hile, M., Halleck, P.M., Mathews, J.P., 2009. Three-dimensional carbon dioxide-induced strain distribution within a confined bituminous coal. Int. J. Coal Geol. 77, 103–108.
Qajar, J., Francois, N., Arns, C.H., 2013. Microtomographic characterization of dissolution-induced local porosity changes including fines migration in carbonate rock. SPE J. 18, 545–562.
Raeini, A.Q., Blunt, M.J., Bijeljic, B., 2012. Modelling two-phase flow in porous media at the pore scale using the volume-of-fluid method. J. Comput. Phys. 231, 5653–5668.
Raeini, A.Q., Blunt, M.J., Bijeljic, B., 2014. Direct simulations of two-phase flow on micro-CT images of porous media and upscaling of pore-scale forces. Adv. Water Resour. 74, 116–126.
Ramandi, H.L., Armstrong, R.T., Mostaghimi, P., 2016a. Micro-CT image calibration to improve fracture aperture measurement. Case Stud. Nondestruct. Test. Eval. 6, 4–13.
Ramandi, H.L., Armstrong, R.T., Mostaghimi, P., Saadatfar, M., Pinczewsk, W.V., 2015. X-ray micro-computed tomography imaging for coal characterization. In: SPE Asia Pacific Unconventional Resources Conference and Exhibition. Society of Petroleum Engineers.
Ramandi, H.L., Mostaghimi, P., Armstrong, R.T., ,2017. Digital rock analysis for accurate prediction of fractured media permeability. J. Hydrol. In press.
Ramandi, H.L., Mostaghimi, P., Armstrong, R.T., Saadatfar, M., Pinczewski, W.V., 2016b. Porosity and permeability characterization of coal: a micro-computed tomography study. Int. J. Coal Geol. 154, 57–68.
Raoof, A., Hassanizadeh, S., 2012. A new formulation for pore-network modeling of two-phase flow. Water Resour. Res. 48.
Raoof, A., Hassanizadeh, S.M., Leijnse, A., 2010. Upscaling transport of adsorbing solutes in porous media: pore-network modeling. UNKNOWN 9, 624–636.
Rhodes, M.E., Bijeljic, B., Blunt, M.J., 2008. Pore-to-field simulation of single-phase transport using continuous time random walks. Adv. Water Resour. 31, 1527–1539.
Robertson, A., 1970. The Interpretation of Geological Factors for Use in Slope Theory, Planning Open Pit Mines. Proceedings, Johannesburg, pp. 55–71.
Ruckenstein, E., Vaidyanathan, A., Youngquist, G., 1971. Sorption by solids with bidisperse pore structures. Chem. Eng. Sci. 26, 1305–1318.
Saadatfar, M., Turner, M., Arns, C., Averdunk, H., Senden, T., Sheppard, A., Sok, R., Pinczewski, W.V., Kelly, J., Knackstedt, M., 2005. Rock Fabric and Texture from Digital Core Analysis. paper ZZ presented at the SPWLA 46th Annual Logging Symposium, New Orleans, Louisiana, June, pp. 26–29.
Saghafi, A., Javanmard, H., Pinetown, K., 2014. Study of coal gas wettability for CO2 storage and CH4 recovery. Geofluids 14, 310–325.
Sakellariou, A., Arns, C.H., Sheppard, A.P., Sok, R.M., Averdunk, H., Limaye, A., Jones, A.C., Senden, T.J., Knackstedt, M.A., 2007. Developing a virtual materials laboratory. Mater. Today 10, 44–51.
Sakurovs, R., Lavrencic, S., 2011. Contact angles in CO 2-water-coal systems at elevated pressures. Int. J. Coal Geol. 87, 26–32.
Schlüter, S., Sheppard, A., Brown, K., Wildenschild, D., 2014. Image processing of multiphase images obtained via X-ray microtomography: a review. Water Resour. Res. 50, 3615–3639.
Scholtès, L., Donzé, F.-V., Khanal, M., 2011. Scale effects on strength of geomaterials, case study: coal. J. Mech. Phys. Solids 59, 1131–1146.
Seidle, J., 2011. Fundamentals of Coalbed Methane Reservoir Engineering. PennWell Books.
Seidle, J.P., Arri, L.E., 1990. Use of conventional reservoir models for coalbed methane simulation. In: CIM/SPE International Technical Meeting. Society of Petroleum Engineers.
Shan, X., Chen, H., 1993. Lattice Boltzmann model for simulating flows with multiple phases and components. Phys. Rev. E 47, 1815.
Shengchu, H., Wenge, L., Guoquan, Z., 2009. Coalbed methane development and utilization in China: status and future development [J]. China Coal 1, 003.
Sheppard, A.P., Sok, R.M., Averdunk, H., 2004. Techniques for image enhancement and segmentation of tomographic images of porous materials. Phys. A Stat. Mech. its Appl. 339, 145–151.
Shi, J.-Q., Durucan, S., Fujioka, M., 2008. A reservoir simulation study of CO 2 injection and N 2 flooding at the Ishikari coalfield CO 2 storage pilot project, Japan. Int. J. Greenh. Gas Control 2, 47–57.
Siemons, N., Bruining, H., Castelijns, H., Wolf, K.-H., 2006. Pressure dependence of the contact angle in a CO 2–H 2 O–coal system. J. Colloid Interface Sci. 297, 755–761.
Simons, F.J., Swennen, R., 1997. Quantitative characterization of coal by means of microfocal X-ray computed microtomography (CMT) and color image analysis (CIA). Int. J. Coal Geol. 34, 69–88.
Song, W., de Haas, T.W., Fadaei, H., Sinton, D., 2014. Chip-off-the-old-rock: the study of reservoir-relevant geological processes with real-rock micromodels. Lab a Chip 14, 4382–4390.
Su, K., Latham, J.P., Pavlidis, D., Xiang, J., Fang, F., Mostaghimi, P., Percival, J.R., Pain, C.C., Jackson, M.D., 2015. Multiphase flow simulation through porous media with explicitly resolved fractures. Geofluids 15, 592–607.
Taber, J.J., Fulton, P., Dabbous, M., 1974. Development of techniques and the measurement of relative permeability and capillary pressure relationships in coal: 30F. US. Bur. Mines, OFR, N22, 1974, 80P. Int. J. Rock Mech. Min. Sci. Geomechanics Abstr. Pergamon 203.
Tahmasebi, P., Javadpour, F., Sahimi, M., 2015. Multiscale and multiresolution modeling of shales and their flow and morphological properties. Sci. Rep. 5.
Tansey, J., Balhoff, M.T., 2016. Pore network modeling of reactive transport and dissolution in porous media. Transp. Porous Media 1–25.
Tartakovsky, A., Meakin, P., 2005. Modeling of surface tension and contact angles with smoothed particle hydrodynamics. Phys. Rev. E 72, 026301.
Tidwell, V.C., Meigs, L.C., Christian-Frear, T., Boney, C.M., 2000. Effects of spatially heterogeneous porosity on matrix diffusion as investigated by X-ray absorption imaging. J. Contam. Hydrol. 42, 285–302.
Towler, B., Firouzi, M., Underschultz, J., Rifkin, W., Garnett, A., Schultz, H., Esterle, J., Tyson, S., Witt, K., 2016. An overview of the coal seam gas developments in Queensland. J. Nat. Gas Sci. Eng. 31, 249–271.
Tsotsis, T.T., Patel, H., Najafi, B.F., Racherla, D., Knackstedt, M.A., Sahimi, M., 2004. Overview of laboratory and modeling studies of carbon dioxide sequestration in coal beds. Ind. Eng. Chem. Res. 43, 2887–2901.
Van Geet, M., Swennen, R., 2001. Quantitative 3D-fracture analysis by means of microfocus X-Ray Computer Tomography (μCT): an example from coal. Geophys. Res. Lett. 28, 3333–3336.
Van Geet, M., Swennen, R., David, P., 2001. Quantitative coal characterisation by means of microfocus X-ray computer tomography, colour image analysis and back-scattered scanning electron microscopy. Int. J. Coal Geol. 46, 11–25.
Vandersteen, K., Busselen, B., Van Den Abeele, K., Carmeliet, J., 2003. Quantitative Characterization of Fracture Apertures Using Microfocus Computed Tomography, vol. 215. Geological Society, London, Special Publications, pp. 61–68.
Varslot, T., Kingston, A., Myers, G., Sheppard, A., 2012. Considerations for high-magnification high-cone-angle helical micro-CT, SPIE Optical Engineering+ Applications. Int. Soc. Opt. Photonics, 850614–850614-850610.
Vega, B., Dutta, A., Kovscek, A.R., 2014. CT imaging of low-permeability, dual-porosity systems using high X-ray contrast gas. Transp. Porous Media 101,

81–97.
Verhelst, F., David, P., Fermont, W., Jegers, L., Vervoort, A., 1996. Correlation of 3D-computerized tomographic scans and 2D-colour image analysis of Westphalian coal by means of multivariate statistics. Int. J. Coal Geol. 29, 1–21.
Verhelst, F., Vervoort, A., De Bosscher, P., Marchal, G., 1995. X-ray computerized tomography: determination of heterogeneities in rock samples. In: 8th ISRM Congress. International Society for Rock Mechanics.
Vincent, L., Soille, P., 1991. Watersheds in digital spaces: an efficient algorithm based on immersion simulations. IEEE Trans. Pattern Anal. Mach. Intell. 13, 583–598.
Vishal, V., Singh, L., Pradhan, S., Singh, T., Ranjith, P., 2013. Numerical modeling of Gondwana coal seams in India as coalbed methane reservoirs substituted for carbon dioxide sequestration. Energy 49, 384–394.
Wei, X., Massarotto, P., Wang, G., Rudolph, V., Golding, S.D., 2010. CO2 sequestration in coals and enhanced coalbed methane recovery: new numerical approach. Fuel 89, 1110–1118.
Wei, X.R., Wang, G.X., Massarotto, P., Golding, S.D., Rudolph, V., 2007. A review on recent advances in the numerical simulation for coalbed-methane-recovery process. SPE Reserv. Eval. Eng. 10, 657–666.
Wildenschild, D., Sheppard, A.P., 2013. X-ray imaging and analysis techniques for quantifying pore-scale structure and processes in subsurface porous medium systems. Adv. Water Resour. 51, 217–246.
Wildenschild, D., Vaz, C., Rivers, M., Rikard, D., Christensen, B., 2002. Using X-ray computed tomography in hydrology: systems, resolutions, and limitations. J. Hydrol. 267, 285–297.
Wolf, K.-H.A., van Bergen, F., Ephraim, R., Pagnier, H., 2008. Determination of the cleat angle distribution of the RECOPOL coal seams, using CT-scans and image analysis on drilling cuttings and coal blocks. Int. J. Coal Geol. 73, 259–272.
Xu, W., Ok, J.T., Xiao, F., Neeves, K.B., Yin, X., 2014. Effect of pore geometry and interfacial tension on water-oil displacement efficiency in oil-wet microfluidic porous media analogs. Phys. Fluids 26 (1994-present), 093102.
Yang, T., Jia, P., Shi, W., Wang, P., Liu, H., Yu, Q., 2014. Seepage–stress coupled analysis on anisotropic characteristics of the fractured rock mass around roadway. Tunn. Undergr. Space Technol. 43, 11–19.
Yao, Y., Liu, D., 2012. Comparison of low-field NMR and mercury intrusion porosimetry in characterizing pore size distributions of coals. Fuel 95, 152–158.
Yao, Y., Liu, D., Che, Y., Tang, D., Tang, S., Huang, W., 2009. Non-destructive characterization of coal samples from China using microfocus X-ray computed tomography. Int. J. Coal Geol. 80, 113–123.
Yao, Y., Liu, D., Che, Y., Tang, D., Tang, S., Huang, W., 2010. Petrophysical characterization of coals by low-field nuclear magnetic resonance (NMR). Fuel 89, 1371–1380.
Young, G., McElhiney, J., Dhir, R., Mavor, M., Anbouba, I., 1991a. Coalbed methane production potential of the rock springs formation, Great divide Basin, Sweetwater County, Wyoming. In: SPE Gas Technology Symposium. Society of Petroleum Engineers.
Young, G., McElhiney, J., Paul, G., McBane, R., 1991b. An analysis of Fruitland coalbed methane production, Cedar Hill field, northern San Juan Basin. In: SPE Annual Technical Conference and Exhibition. Society of Petroleum Engineers.
Yu, Y., Liang, W., Hu, Y., Meng, Q., 2012. Study of micro-pores development in lean coal with temperature. Int. J. Rock Mech. Min. Sci. 51, 91–96.
Zhang, J., Feng, Q., Zhang, X., Wen, S., Zhai, Y., 2015. Relative permeability of coal: a review. Transp. Porous Media 106, 563–594.
Zhang, X., Wang, K., Wang, A., Gong, P., 2016a. Analysis of internal pore structure of coal by micro-computed tomography and mercury injection. Int. J. Oil, Gas Coal Technol. 12, 38–50.
Zhang, Y., Lebedev, M., Sarmadivaleh, M., Barifcani, A., Iglauer, S., 2016b. Swelling-induced changes in coal microstructure due to supercritical CO2 injection. Geophys. Res. Lett. 43, 9077–9083.
Zhang, Y., Lebedev, M., Sarmadivaleh, M., Barifcani, A., Rahman, T., Iglauer, S., 2016c. Swelling effect on coal micro structure and associated permeability reduction. Fuel 182, 568–576.